Nonparametric Modern Hopfield Models

Jerry Yao-Chieh Hu[†*1], Bo-Yu Chen[‡*2], Dennis Wu[†3], Feng Ruan[§4], Han Liu[†§5]

† Department of Computer Science, Northwestern University, Evanston, IL 60208, USA
‡ Department of Physics, National Taiwan University, Taipei 10617, Taiwan
§ Department of Statistics and Data Science, Northwestern University, Evanston, IL 60208, USA

We present a nonparametric construction for deep learning compatible modern Hopfield models and utilize this framework to debut an efficient variant. Our key contribution stems from interpreting the memory storage and retrieval processes in modern Hopfield models as a nonparametric regression problem subject to a set of query-memory pairs. Crucially, our framework not only recovers the known results from the original dense modern Hopfield model but also fills the void in the literature regarding efficient modern Hopfield models, by introducing *sparse-structured* modern Hopfield models with sub-quadratic complexity. We establish that this sparse model inherits the appealing theoretical properties of its dense analogue — connection with transformer attention, fixed point convergence and exponential memory capacity — even without knowing details of the Hopfield energy function. Additionally, we showcase the versatility of our framework by constructing a family of modern Hopfield models as extensions, including linear, random masked, top-K and positive random feature modern Hopfield models. Empirically, we validate the efficacy of our framework in both synthetic and realistic settings.

---

[1] jhu@u.northwestern.edu
[2] b12202023@ntu.edu.tw
[3] hibb@u.northwestern.edu
[4] fengruan@northwestern.edu
[5] hanliu@northwestern.edu
*These authors contributed equally to this work. Code is available at GitHub.

Contents

1 Introduction

We tackle the challenges in computational efficiency of modern Hopfield models [Wu et al., 2024b, Hu et al., 2023, Ramsauer et al., 2020] by presenting a nonparametric framework, and then debuting the first (to our knowledge) efficient modern Hopfield model with sub-quadratic complexity and appealing theoretical properties. Such a construction is of practical importance. As in many Hopfield-centric methods [Hu et al., 2024a, Wu et al., 2024a, Xu et al., 2024, Wu et al., 2024b, Schimunek et al., 2023, Fürst et al., 2022, Paischer et al., 2022, Seidl et al., 2022, Widrich et al., 2020], modern Hopfield models (and their derived deep learning layers) serve as powerful alternatives to the attention mechanism with additional functionalities, but lack efficient implementation for gigantic deep models [Hu et al., 2023, Section C.2]. This issue becomes more prominent in this era of Large Foundation Models [Bommasani et al., 2021]. Foundation models huge attention-based models pretrained on massive datasets, and play a central role not only in machine learning but also in a wide range of scientific domains, such as ChatGPT [Brown et al., 2020, Floridi and Chiriatti, 2020] for natural language, BloombergGPT [Wu et al., 2023] for finance, DNABERT [Zhou et al., 2024a,b, Ji et al., 2021] for genomics, and many others. To push toward Hopfield-based large foundation models, this work provides a timely efficient solution, back-boned by a solid theoretical ground.

Modern Hopfield models [Ramsauer et al., 2020], motivated by the dense associative memory models [Demircigil et al., 2017, Krotov and Hopfield, 2016], are (auto-)associative memory models that (i) have exponential memory capacity, (ii) retrieve stored patterns based on input queries with only one retrieval step, and (iii) are compatible with deep learning architectures. They achieve (i) by adopting highly non-linear energy functions, (ii) by adopting a memory-retrieval dynamics ensuring monotonic minimization of the energy function, and (iii) by the connection between their memory retrieval dynamics and attention mechanism. Deepening (ii) and (iii), Hu et al. [2023] and Wu et al. [2024b] propose a theoretical framework for deriving modern Hopfield models using various entropic regularizers. In addition, they introduce a sparse extension of the original modern Hopfield model to handle its computational burden and vulnerability to noise. As a result, their proposal not only connects to sparse attention mechanism [Correia et al., 2019, Martins and Astudillo, 2016] but also offers both provably computational advantages and robust empirical performance.

However, there are still some missing pieces toward a unified theoretical framework for modern Hopfield models:

- **(P1) Lack of Efficiency.** Computationally, while Hu et al. [2023] and Wu et al. [2024b] indeed introduce sparsity into their model, this sparsity does not implies computational efficiency. In fact, it only increases efficiency at the level of memory retrieval, (i.e. the sparsity in [Hu et al., 2023, Wu et al., 2024b] only leads to faster memory retrieval but not

necessarily shorter running time, as discussed in [Hu et al., 2023, Section C.2]). Namely, the sparse modern Hopfield model still suffers by the $\mathcal{O}(n^2)$ complexity (with the input sequence length n), which hampers its scalability[1].

- **(P2) Lack of Rigorous Analysis on Sparsity.** Theoretically, because Hu et al. [2023] choose not to make strong assumptions (on the memory and query patterns) in order to maintain their model's generality, they only offer qualitative justifications [Hu et al., 2023, Section 3]. They do not rigorously characterize how sparsity impacts different aspects of the sparse model, e.g., the retrieval error, the well-separation condition, and the memory capacity.

- **(P3) Incomplete Connection between Attention and Hopfield Models.** Methodologically, while numerous variants of the attention module exist [Choromanski et al., 2021, Katharopoulos et al., 2020, Beltagy et al., 2020, Child et al., 2019], Hu et al. [2023] only bridge a subset of them to modern Hopfield models. A natural question arises: How can we integrate the advancements of state-of-the-art attention into modern Hopfield models? As noted in [Hu et al., 2024b, 2023, Wu et al., 2024b], this question is far from trivial. Naively substituting the softmax activation function with other alternatives does not necessarily yield well-defined Hopfield models and might sabotage their desirable properties and functionalities.

To fill these gaps, this work presents a nonparametric framework for deep learning compatible modern Hopfield models. To fill **(P1)**, this framework allows us to not only recover the standard dense modern Hopfield model [Ramsauer et al., 2020], but also introduce an efficient modern Hopfield model, termed sparse-structured modern Hopfield model (Theorem 3.2). To fill **(P2)**, our framework facilitates the derivation of a retrieval error bound of the sparse modern Hopfield with explicit sparsity dependence (Theorem 4.1). This bound offers rigorous characterizations of the sparsity-induced advantages of the sparse model compared with its dense counterpart, including higher precision in memory retrieval (Corollary 4.1.1 and Corollary 4.1.2), enhanced robustness to noise (Remark 4.2) and exponential-in-d capacity (Theorem 4.2 and Lemma 4.2, d refers to pattern size). Interestingly, unlike existing Hopfield models [Hu et al., 2023, Wu et al., 2023, Ramsauer et al., 2020] requiring an explicit energy function to guarantee the stability of the model, we show that the sparse modern Hopfield model guarantees the fixed-point convergence even without details of the Hopfield energy function (Lemma 4.1). To fill **(P3)**, beyond introducing the sparse modern Hopfield model, our framework supports a family of modern Hopfield models that connect with various attention variants. This complements the findings in [Hu et al., 2023, Wu et al., 2024b], pushing us toward a more unified understanding.

Contributions. Our contributions are as follows:

---

[1]See Remark 3.7 for the connection between time complexity of attention and of modern Hopfield models.

- We propose a nonparametric framework for deep learning compatible modern Hopfield models. Building upon this, we introduce the first efficient sparse modern Hopfield model with sub-quadratic complexity.

- We provide rigorous characterizations of the sparsity-induced advantages of the proposed efficient model: tighter retrieval error bound (Corollary 4.1.1 and Corollary 4.1.2), stronger noise robustness (Remark 4.2) and exponential-d-capacity (Theorem 4.2 and Lemma 4.2).

- Based on the proposed framework, we construct a family of modern Hopfield models connecting to many existing attention variants [Choromanski et al., 2021, Zaheer et al., 2020, Beltagy et al., 2020, Katharopoulos et al., 2020], and verify their efficacy through thorough numerical experiments in both synthetic and realistic settings.

Related Works

Modern Hopfield Models for Deep Learning. The classical Hopfield models [Hopfield, 1984, 1982, Krotov and Hopfield, 2016] are canonical models of the human brain's associative memory. Their primary function is the storage and retrieval of specific memory patterns. Recently, a resurgence of interest in Hopfield models within the machine learning field is attributed to developments in understanding memory storage capacities [Krotov and Hopfield, 2016, Demircigil et al., 2017, Wu et al., 2024a], innovative architecture [Hoover et al., 2023, Seidl et al., 2022, Fürst et al., 2022, Ramsauer et al., 2020], and their biological plausibility [Kozachkov et al., 2022, Krotov and Hopfield, 2021]. Notably, the modern Hopfield models [Wu et al., 2024b, Hu et al., 2023, Ramsauer et al., 2020, Brandstetter, 2021], demonstrate not only a strong connection to the transformer attention mechanisms in deep learning, but also superior performance, and a theoretically guaranteed exponential memory capacity. In this regard, seeing the modern Hopfield models as an advanced extension of attention mechanisms opens up prospects for crafting Hopfield-centric architectural designs. Therefore, their applicability spans diverse areas like drug discovery [Schimunek et al., 2023], immunology [Widrich et al., 2020], tabular learning [Xu et al., 2024], time series forecasting [Wu et al., 2024b, Auer et al., 2024], reinforcement learning [Paischer et al., 2022], and large foundation models [Hu et al., 2024a, Fürst et al., 2022]. This work emphasizes refining this line of research towards efficient models. We posit that this effort is crucial in guiding future research towards Hopfield-driven design paradigms, especially for larger models.

Sparse Modern Hopfield Model. [Ramsauer et al., 2020] establish a connection between Hopfield models and the vanilla softmax attention. Motivated by this connection, [Hu et al., 2023, Wu et al., 2024b] (and later [Martins et al., 2023]) propose a theoretical framework for modern Hopfield models based on the relationship between entropic regularizers and finite-domain distributions with varying support sets. Importantly, they not only show that [Ramsauer et al., 2020] is

just special case within their framework but also propose a sparse extension with superior properties (e.g., robust representation learning, fast fixed-point convergence, and exponential memory capacity) and connection to certain types of sparse attention. However, this is not end of the story. As highlighted in [Hu et al., 2023, Section E], their framework only bridges a subset of existing attention variants (with dense quadratic attention score matrix) and hence is not complete. This work fills this theoretical gap by providing a principle construction for the many modern Hopfield models with theoretical guarantees. Moreover, our framework supports a family of modern Hopfield models mirroring many popular structured efficient attention mechanisms, including Attention with Pre-defined Patterns (each sequence token attends to a predetermined subset of tokens instead of the entire sequence, e.g, Big Bird [Zaheer et al., 2020], Longformer [Beltagy et al., 2020], Blockwise [Qiu et al., 2019], Sparse [Child et al., 2019]), and Kernelized Attention (e.g., Performer [Choromanski et al., 2021], Linear [Clevert et al., 2015] and Multi-head [Vaswani et al., 2017]).

Notations. We denote vectors by lower case bold letters, and matrices by upper case bold letters. We write $\langle \mathbf{a}, \mathbf{b} \rangle := \mathbf{a}^\mathsf{T} \mathbf{b}$ as the inner product for vectors $\mathbf{a}, \mathbf{b}$. Let $\mathbf{a}[i]$ denotes the i-th element of vector $\mathbf{a}$. The index set $\{1, \cdots, I\}$ is denoted by $[I]$, where $I \in \mathbb{N}_+$. The spectral norm is denoted by $\|\cdot\|$, which is equivalent to the l_2-norm when applied to a vector. We denote the memory patterns by $\boldsymbol{\xi} \in \mathbb{R}^d$ and the query pattern by $\mathbf{x} \in \mathbb{R}^d$, and $\boldsymbol{\Xi} := [\boldsymbol{\xi}_1, \cdots, \boldsymbol{\xi}_M] \in \mathbb{R}^{d \times M}$ as shorthand for stored memory patterns $\{\boldsymbol{\xi}_\mu\}_{\mu \in [M]}$. Moreover, we set $m := \mathrm{Max}_{\mu \in [M]} \|\boldsymbol{\xi}_\mu\|$ be the largest norm of memory patterns.

Organization. Section 2 reviews modern Hopfield models. Section 3 presents a nonparametric construction for modern Hopfield models, and debut the sparse-structured (efficient) modern Hopfield models. Section 4 provides the theoretical analysis on the sparse-structured modern Hopfield models. Appendix C includes a family of modern Hopfield models as possible extensions. We conduct numerical experiments to support our framework in Appendix E.

2 Background: Modern Hopfield Models

This section presents the ideas we build on.

2.1 Soft-Margin Support Vector Regression

Soft-margin Support Vector Regression (SVR) [Awad et al., 2015, Jaggi, 2014] aims to fit the best hyperplane (in the higher dimensional feature space) to the data, within a certain margin of error tolerance ϵ', while allowing controllable flexibility (*softened* margin) for data points that are outside this margin. Given a feature map $\Phi : \mathbb{R}^d \to \mathbb{R}^{D_\Phi}$, a training dataset $\{(\mathbf{x}_\mu, \mathbf{y}_\mu)\}_{\mu=1}^M$, where

$\mathbf{x}_\mu \in \mathbb{R}^d$ is a feature vector and $\mathbf{y}_\mu \in \mathbb{R}^d$ is the target output, the objective of SVR is to find a function $f(\mathbf{x}) = \mathbf{W}\Phi(\mathbf{x}) + \mathbf{b}$ that has at most ϵ'-deviation from the actual targets $\mathbf{y}_\mu$ for all the data points, with $\mathbf{W} := [\mathbf{w}_1, \ldots, \mathbf{w}_d]^\mathsf{T} \in \mathbb{R}^{d \times D_\Phi}$ being the weight matrix, and $\mathbf{b} \in \mathbb{R}^d$ the bias term. The soft-margin SVR formulation introduces slack variables $\boldsymbol{\eta}_\mu, \widetilde{\boldsymbol{\eta}}_\mu \geq 0$ to handle constraints that might otherwise be infeasible due to data noise. The soft-margin SVR with squared loss (ℓ_2-loss) is formulated as:

$$\min_{\mathbf{W}, \boldsymbol{\eta}, \widetilde{\boldsymbol{\eta}}} \frac{1}{2} \|\mathbf{W}\|^2 + C \sum_{\mu=1}^{M} \langle \mathbb{1}, (\boldsymbol{\eta}_\mu + \widetilde{\boldsymbol{\eta}}_\mu) \rangle \tag{2.1}$$

$$\text{subject to} \begin{cases} \mathbf{y}_\mu - \langle \mathbf{W}, \Phi(\mathbf{x}_\mu) \rangle - \mathbf{b} \leq \epsilon' \mathbb{1} + \boldsymbol{\eta}, \\ \langle \mathbf{W}, \Phi(\mathbf{x}_\mu) \rangle + \mathbf{b} - \mathbf{y}_\mu \leq \epsilon' \mathbb{1} + \widetilde{\boldsymbol{\eta}}, \\ \boldsymbol{\eta}_\mu, \widetilde{\boldsymbol{\eta}}_\mu \geq 0, \quad \mu \in [M], \end{cases}$$

where $C > 0$ is a penalty coefficient that balances the trade-off between the accuracy of $f(\mathbf{x})$ and the extent to which deviations greater than ϵ' are permitted. As (2.1) is strongly convex, there exists a unique minimizer.

Solving this optimization problem involves constructing a Lagrangian with dual variables for each constraint,

$$\begin{aligned} \mathcal{L} := & \frac{1}{2} \sum_{i=1}^{d} \|\mathbf{w}_i\|^2 + C \sum_{\mu=1}^{M} \sum_{i=1}^{d} (\boldsymbol{\lambda}_\mu[i]\boldsymbol{\eta}_\mu[i] + \widetilde{\boldsymbol{\lambda}}_\mu[i]\widetilde{\boldsymbol{\eta}}_\mu[i]) \\ & - \sum_{\mu=1}^{M} \sum_{i=1}^{d} \boldsymbol{\alpha}_\mu[i] \left(\epsilon' + \boldsymbol{\eta}_\mu[i] - \mathbf{y}_\mu[i] + \langle \mathbf{w}_i, \Phi(\mathbf{x}_\mu) \rangle + \mathbf{b}[i] \right) \\ & - \sum_{\mu=1}^{M} \sum_{i=1}^{d} \widetilde{\boldsymbol{\alpha}}_\mu[i] \left(\epsilon' + \widetilde{\boldsymbol{\eta}}_\mu[i] - \langle \mathbf{w}_i, \Phi(\mathbf{x}_\mu) \rangle - \mathbf{b}[i] + \mathbf{y}_\mu[i] \right), \end{aligned}$$

where $\mathbf{a}[i]$ denotes the i-th element of a vector $\mathbf{a}$, $\boldsymbol{\lambda}_\mu, \widetilde{\boldsymbol{\lambda}}_\mu, \boldsymbol{\alpha}_\mu$ and $\widetilde{\boldsymbol{\alpha}}_\mu$ are Lagrange multipliers; and then use Karush-Kuhn-Tucker (KKT) conditions to find the optimal solution.

2.2 Modern Hopfield Models

Let $\mathbf{x} \in \mathbb{R}^d$ be the input query pattern and $\Xi = [\boldsymbol{\xi}_1, \cdots, \boldsymbol{\xi}_M] \in \mathbb{R}^{d \times M}$ the M memory patterns.

Hopfield Models. The aim of Hopfield models [Hopfield, 1982, 1984] is to store these memory patterns Ξ and retrieve a specific memory $\boldsymbol{\xi}_\mu$ when given a query $\mathbf{x}$. They achieve these by embedding the memories in the energy landscape $E(\mathbf{x})$ of a physical system, where each memory

$\boldsymbol{\xi}_\mu$ corresponds to a local minimum. When a query $\mathbf{x}$ is presented, the model initiates energy-minimizing retrieval dynamics $\mathcal{T}$ at the query, which then navigate the energy landscape to find the nearest local minimum, effectively retrieving the memory most similar to the query.

These models comprise two primary components: an *energy function* $E(\mathbf{x})$ that encodes memories into its local minima, and a *retrieval dynamics* $\mathcal{T}(\mathbf{x})$ that fetches a memory by iteratively minimizing $E(\mathbf{x})$ starting with a query.

Constructing the energy function, $E(\mathbf{x})$, is straightforward. As outlined in [Krotov and Hopfield, 2016], memories get encoded into $E(\mathbf{x})$ using the *overlap-construction*: $E(\mathbf{x}) = F(\boldsymbol{\Xi}^\mathsf{T}\mathbf{x})$, where $F : \mathbb{R}^M \to \mathbb{R}$ is a smooth function. This ensures that the memories $\{\boldsymbol{\xi}_\mu\}_{\mu \in [M]}$ sit at the stationary points of $E(\mathbf{x})$, i.e. $\nabla_\mathbf{x} F(\boldsymbol{\Xi}^\mathsf{T}\mathbf{x})|_{\boldsymbol{\xi}_\mu} = 0$ for all $\mu \in [M]$. The choice of F results in different Hopfield model types, as demonstrated in [Krotov and Hopfield, 2016, Demircigil et al., 2017, Ramsauer et al., 2020, Krotov and Hopfield, 2021]. However, determining a suitable retrieval dynamics, $\mathcal{T}$, for a given energy $E(\mathbf{x})$ is more challenging. For effective memory retrieval, $\mathcal{T}$ must:

(T1) Monotonically reduce $E(\mathbf{x})$ when applied iteratively.

(T2) Ensure its fixed points coincide with the stationary points of $E(\mathbf{x})$ for precise retrieval.

Modern Hopfield Models. Ramsauer et al. [2020] propose the modern Hopfield model with a specific set of E and $\mathcal{T}$ satisfying above requirements, and integrate it into deep learning architectures via its strong connection with attention mechanism, offering enhanced performance, and theoretically guaranteed exponential memory capacity. Specifically, they introduce the energy function:

$$E(\mathbf{x}) = -\operatorname{lse}(\beta, \boldsymbol{\Xi}^\mathsf{T}\mathbf{x}) + \frac{1}{2}\langle\mathbf{x}, \mathbf{x}\rangle, \tag{2.2}$$

where the retrieval dynamics is given by

$$\mathbf{x}^{\text{new}} = \mathcal{T}_{\text{Dense}}(\mathbf{x}) = \boldsymbol{\Xi} \cdot \operatorname{Softmax}(\beta\boldsymbol{\Xi}^\mathsf{T}\mathbf{x}). \tag{2.3}$$

The function $\operatorname{lse}(\beta, \mathbf{z}) := \log\left(\sum_{\mu=1}^M \exp\{\beta z_\mu\}\right)/\beta$ is the log-sum-exponential for any given vector $\mathbf{z} \in \mathbb{R}^M$ and $\beta > 0$. Their analysis reveals that:

(i) The $\mathcal{T}_{\text{Dense}}$ dynamics converge well (T2) and can retrieve patterns accurately in just one step (T1).

(ii) The modern Hopfield model from (2.2) possesses an exponential memory capacity in pattern size d.

(iii) Notably, the one-step approximation of $\mathcal{T}_{\text{Dense}}$ mirrors the attention mechanism in transformers, leading to a novel deep learning architecture design: the Hopfield layers.

Attention ↔ Modern Hopfield Model. To see above (iii), suppose that $\mathbf{X}$ and $\mathbf{\Xi}$ are embedded from the *raw* query $\mathbf{R}$ and $\mathbf{Y}$ memory patterns, respectively, via $\mathbf{X}^{\mathsf{T}} = \mathbf{R}\mathbf{W}_Q := \mathbf{Q}$, and $\mathbf{\Xi}^{\mathsf{T}} = \mathbf{Y}\mathbf{W}_K := \mathbf{K}$, with some projection matrices $\mathbf{W}_Q$ and $\mathbf{W}_K$. Then, taking the transpose of $\mathcal{T}$ in (2.3) and multiplying with $\mathbf{W}_V$ such that $\mathbf{V} := \mathbf{K}\mathbf{W}_V$, we obtain

$$\mathbf{Z} := \mathbf{Q}^{\text{new}}\mathbf{W}_V = \text{Softmax}\left(\beta\mathbf{Q}\mathbf{K}^{\mathsf{T}}\right)\mathbf{V}. \tag{2.4}$$

This enables modern Hopfield models to serve as alternatives to attention mechanism with extra functionalities.

Given the equivalence (2.4), one might wonder if the quest for efficient modern Hopfield models is equivalent to seeking efficient attention mechanisms [Tay et al., 2022], specifically in terms of finding efficient implementations of the Softmax matrix computation. We contend that they are not the same. To build a modern Hopfield model, we expect not only its retrieval dynamics to connect to attention mechanism, but also it to serve as an associative memory model [Hu et al., 2024a, Wu et al., 2024b, Hu et al., 2023, Ramsauer et al., 2020] by design. Moreover, we observe that (T1) and (T2) are essentially about encoding memories onto the fixed points of $\mathcal{T}$.

These motivate us to view the construction of $\mathcal{T}$ as a learning problem: we aim to learn a function $\mathcal{T}$ satisfying (T2) from a dataset consisting of query-memory pairs. Thus, rather than using the traditional Hopfield model's learning rule — where the model memorizes memories by defining an energy function, like the overlap-construction [Hu et al., 2023] — we interpret the memorization process as learning a function that maps queries to memories. This new perspective allows us to construct novel modern Hopfield models that are equivalent to various attention variants.
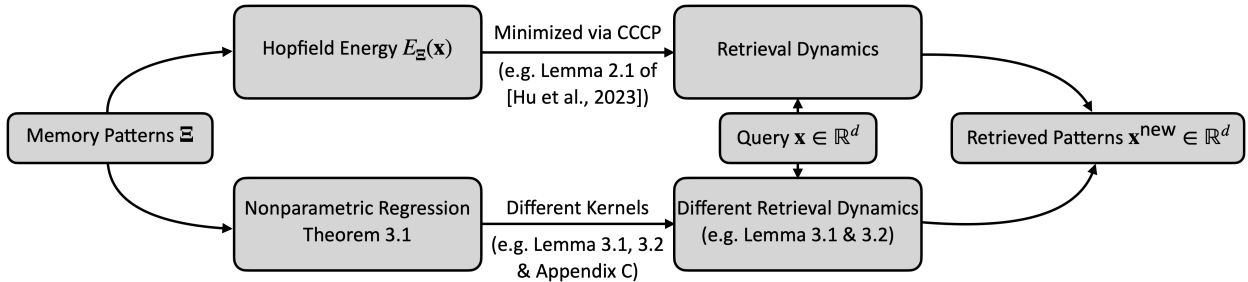
3 Nonparametric Modern Hopfield Models

Figure 1: A High-level Visualization

Overview of Our Framework.

8

- In Section 3.1, we formulate the memory storage and retrieval of modern Hopfield models as a nonparametric regression problem. We first align the definition of $\mathcal{T}$ (the retrieval dynamics (2.3)) with a nonparametric regression problem subject to a set of query-memory pairs. Then, by solving for optimality, we derive a nonparametric formulation of $\mathcal{T}$. We provide a high-level visualization of our framework in Figure 1.

- In Section 3.2, we showcase our framework with two special cases: the standard dense modern Hopfield model [Ramsauer et al., 2020] (Lemma 3.1), and a new, efficient sparse-structured modern Hopfield model (Theorem 3.2).

3.1 Retrieval Dynamics

The retrieval dynamics (2.3) $\mathcal{T}_{\Xi}(\mathbf{x}) : \mathbb{R}^d \to \mathbb{R}^d$ maps an input query $\mathbf{x}$ to $\mathcal{T}_{\Xi}(\mathbf{x})$, with the aim of retrieving the memory pattern $\boldsymbol{\xi}_\mu$ closest to $\mathbf{x}$. To formalize this notion of retrieval, we need a few definitions and notation.

Definition 3.1 (Generalized Fixed Point [Sriperumbudur and Lanckriet, 2009]). We say a set $\mathcal{S} \subseteq \mathbb{R}^d$ a *generalized fixed point* with respect to $\mathcal{T}_{\Xi}$ if $\mathcal{T}_{\Xi}(\mathbf{y}) \in \mathcal{S}$ for every $\mathbf{y} \in \mathcal{S}$.

Remark 3.1 (Fixed Point). In contrast to Definition 3.1, a fixed point of $\mathcal{T}_{\Xi}$ is a point $\mathbf{y}$ for which $\mathcal{T}_{\Xi}(\mathbf{y}) = \mathbf{y}$.

Remark 3.2. A generalized fixed point $\mathcal{S}$ with respect to $\mathcal{T}_{\Xi}$ is also an *invariant set* with respect to $\mathcal{T}_{\Xi}$.

In particular, if the retrieval dynamics is initiated at $\mathbf{x} \in \mathcal{S}$ where $\mathcal{S}$ is an invariant set, then subsequent iterates such as $\mathcal{T}_{\Xi}(\mathbf{x}), \mathcal{T}_{\Xi} \circ \mathcal{T}_{\Xi}(\mathbf{x}), \ldots$ remain in the invariant set $\mathcal{S}$.

Now we introduce a neighborhood — $\mathcal{S}_\mu$, a ball of radius R — at every memory pattern $\boldsymbol{\xi}_\mu$:

$$\mathcal{S}_\mu = \{\boldsymbol{\xi} \mid \|\boldsymbol{\xi} - \boldsymbol{\xi}_\mu\| \leq R\},$$

where

$$R := \frac{1}{2} \min_{\mu,\nu \in [M]; \mu \neq \nu} \|\boldsymbol{\xi}_\mu - \boldsymbol{\xi}_\nu\|.$$

By definition, neighborhoods associated with distinct memory patterns do not overlap: $\mathcal{S}_\mu \cap \mathcal{S}_\nu = \emptyset$ for $\mu \neq \nu$. To measure the progress of the dynamics in retrieving the memory pattern, we introduce the notion of memory storage and ϵ-retrieval.

Definition 3.2 (Storage and ϵ-Retrieval). A memory pattern $\boldsymbol{\xi}_\mu$ is *stored* if $\mathcal{S}_\mu$ is a generalized fixed point of $\mathcal{T}$. A memory pattern $\boldsymbol{\xi}_\mu$ gets ϵ-*retrieved* by $\mathcal{T}_{\Xi}$ with an input query $\mathbf{x}$ if $\|\mathcal{T}_{\Xi}(\mathbf{x}) - \boldsymbol{\xi}_\mu\| \leq \epsilon$.

In below, when the context is clear, we suppress the notation dependence of $\mathcal{T}_{\Xi}$ on the memory patterns Ξ for simplicity.

Definition 3.2 states that for an input $\mathbf{x}$ around a stored memory pattern $\boldsymbol{\xi}$, its corresponding mapping output $\mathcal{T}(\mathbf{x})$ should be located in the same sphere $\mathcal{S}$. This motivates us to view $\mathcal{T}$ as a function aiming to map the query $\mathbf{x}$ onto its nearest memory $\boldsymbol{\xi}$ within an error-tolerance margin R. More precisely, in this work, we construct such a function satisfying Definition 3.2 as a learning problem, using memory patterns as data. A natural choice for doing this function is through the soft-margin SVR (see Section 2.1): it fits the best hyperplane to the data points within a predefined error margin, aiming to minimize the error rate while ensuring the model remains insensitive to errors within a certain threshold.

We first define the regression model. Given a weight matrix $\mathbf{W} \in \mathbb{R}^{d \times D_{\Phi}}$, and a feature map $\Phi : \mathbb{R}^d \to \mathbb{R}^{D_{\Phi}}$, denote $f_{W,\Phi} : \mathbb{R}^d \to \mathbb{R}^d$ to be the mapping

$$f_{W,\Phi}(\mathbf{x}) = \mathbf{W}\Phi(\mathbf{x}). \tag{3.1}$$

Denote $\mathcal{K}(x_1, x_2) := \langle \Phi(x_1), \Phi(x_2) \rangle$. This is a positive semidefinite kernel, and there is a unique RKHS $\mathcal{H}$ that is associated with this kernel $\mathcal{K}$ [Wainwright, 2019, Theorem 12.11].

To cast $\mathcal{T}$ as a SVR problem using (3.1), we now specify the data points that $f(\mathbf{x})$ should fit. Since the goal of $\mathcal{T}$ is to retrieve the memory pattern most similar to given query $\mathbf{x}$, we consider the training dataset $\mathcal{D} = \{(\boldsymbol{\xi}_{\mu} + \delta\boldsymbol{\xi}_{\mu}, \boldsymbol{\xi}_{\mu})\}_{\mu \in [M]}$. Namely, the input query $\mathbf{x} = \boldsymbol{\xi}_{\mu} + \delta\boldsymbol{\xi}_{\mu}$ is the contaminated target memory pattern with noise $\delta\boldsymbol{\xi}_{\mu}$, and the output $\mathbf{y} = \boldsymbol{\xi}_{\mu}$ is target memory pattern. For convenience, we shorthand $[\boldsymbol{\xi}_1 + \delta\boldsymbol{\xi}_1, \cdots, \boldsymbol{\xi}_M + \delta\boldsymbol{\xi}_M] = \Xi_{\delta} \in \mathbb{R}^{d \times M}$ as the contaminated memory patterns.

Next, we frame the memorization in modern Hopfield models as fitting f to the dataset $\mathcal{D}$, and obtain the following nonparametric (support vector) regression problem.

Given a dataset $\mathcal{D} = \{(\boldsymbol{\xi}_{\mu} + \delta\boldsymbol{\xi}_{\mu}, \boldsymbol{\xi}_{\mu})\}_{\mu \in [M]}$, consider the support vector regression using the feature map Φ

$$\underset{\mathbf{W}, \boldsymbol{\eta}, \widetilde{\boldsymbol{\eta}}}{\text{Min}} \frac{1}{2} \|\mathbf{W}\|^2 + C \sum_{\mu=1}^{M} \langle \mathbb{1}, (\boldsymbol{\eta}_{\mu} + \widetilde{\boldsymbol{\eta}}_{\mu}) \rangle \tag{3.2}$$

subject to

$$
\begin{cases}
-(\epsilon'\mathbb{1} + \widetilde{\boldsymbol{\eta}}_\mu) \leq \boldsymbol{\xi}_\mu - \langle \mathbf{W}, \Phi(\boldsymbol{\xi}_\mu + \delta\boldsymbol{\xi}_\mu) \rangle \leq \epsilon'\mathbb{1} + \boldsymbol{\eta}_\mu \\
\epsilon'\mathbb{1} + \boldsymbol{\eta}_\mu \leq \epsilon\mathbb{1}/\sqrt{d} \\
\boldsymbol{\eta}_\mu \geq 0, \widetilde{\boldsymbol{\eta}}_\mu \geq 0, \forall\mu \in [M],
\end{cases}
$$

where $\epsilon' > 0$ is a component-wise error margin, $C \geq 0$ is a penalty coefficient, and $\epsilon > 0$ is the memory retrieval error. We denote the unique (given the strong convexity of the optimization problem (3.2)) minimizer as $(\mathbf{W}^*_\Phi, \boldsymbol{\eta}^*_\Phi, \widetilde{\boldsymbol{\eta}}^*_\Phi)$, and the solution to (3.2) as $\mathcal{T}_{\mathrm{SVR}}(\mathbf{x})$. By solving the optimality via the Lagrangian duality, we obtain the following.

Theorem 3.1. Let $\boldsymbol{\alpha}, \widetilde{\boldsymbol{\alpha}}$ denote the Lagrangian multipliers of the dual problem of (3.2). Let $\mathbf{W}^\star := (\mathbf{w}^\star_1, \dots \mathbf{w}^\star_d)^\mathsf{T} \in \mathbb{R}^{d \times D_\Phi}$ denote the minimizer of (3.2). Then,

$$
\mathbf{w}^\star_i = \sum_{\mu=1}^{M} \underbrace{(\boldsymbol{\alpha}_\mu[i] - \widetilde{\boldsymbol{\alpha}}_\mu[i])}_{\in \mathbb{R}} \underbrace{\Phi(\boldsymbol{\xi}_\mu + \delta\boldsymbol{\xi}_\mu)}_{\in \mathbb{R}^{D_\Phi}}, \tag{3.3}
$$

where $\mathbf{a}[i]$ denotes the i-th element of a vector $\mathbf{a}$.

Proof. See Appendix B.1 for a detailed proof. $\qquad\square$

For any featurization map Φ, Theorem 3.1 introduces a map

$$
\mathcal{T}_{\mathrm{SVR},\Phi} := f_{\mathbf{W}^*_\Phi, \Phi}.
$$

By construction, for any Φ, $\mathcal{T}_{\mathrm{SVR},\Phi}$ obeys the ϵ-retrieval property $\|\mathcal{T}_{\mathrm{SVR},\Phi}(x) - \boldsymbol{\xi}_\mu\| \leq \epsilon$, for any μ and $\mathbf{x} \in \mathcal{S}_\mu$. Hence, we arrive a nonparametric framework for constructing many modern Hopfield models. Given an input query $\mathbf{x}$, the i-th component of the retrieved pattern by applying $\mathcal{T}_{\mathrm{SVR}}(\mathbf{x})$ once is

$$
\mathbf{x}^{\mathrm{new}}[i] := \mathcal{T}_{\mathrm{SVR}}(\mathbf{x})[i] = \langle \mathbf{w}^\star_i, \Phi(\mathbf{x}) \rangle. \tag{3.4}
$$

Remark 3.3. Note that ϵ' is the component-wise SVR error, *not* the ϵ in Hopfield retrieval error defined in Definition 3.2.

Remark 3.4. Without any assumption on ϵ, $\mathcal{T}_{\mathrm{SVR}}$ converges to *generalized* fixed points, in contrast to the fixed point convergence in [Hu et al., 2023, Ramsauer et al., 2020]. Thus, there is no multiple update convergence for $\mathcal{T}_{\mathrm{SVR}}$ without specifying Φ (and thereby proving the fixed point convergence property.) We provide specific Φ with provably fixed point convergence in Section 3.2 and Remark 4.3.

Remark 3.5. This regression problem is nonparametric. That is, it does not assume a specific functional form for $\mathcal{T}_{\text{SVR}}$ and is flexible in the number of parameters, allowing the number of support vectors to adjust based on the data.

Intuitively, this optimization problem learns a $\mathcal{T}_{\text{SVR},\Phi}$ to replace $\mathcal{T}$ from the training dataset $\mathcal{D} = \{(\boldsymbol{\xi}_\mu + \delta\boldsymbol{\xi}_\mu, \boldsymbol{\xi}_\mu)\}_{\mu \in [M]}$. Thus, for any given query $\boldsymbol{\xi}_\mu + \delta\boldsymbol{\xi}_\mu$, $\mathcal{T}_{\text{SVR},\Phi}$ retrieves a target memory pattern $\boldsymbol{\xi}_\mu$ with ϵ precision, for all $\mu \in [M]$. Specifically, this ϵ precision comes from the upper bound of the maximum component-wise error $\epsilon' + \boldsymbol{\eta}_\mu[i]$ (and $\epsilon' + \widetilde{\boldsymbol{\eta}}_\mu[i]) \leq \epsilon/\sqrt{d}$, defined in (3.2). This choice of SVR error margin mimics the ϵ-retrieval of modern Hopfield models via the flexibility of soft-margin SVR. As a result, the objective of the SVR problem (3.2) coincides with the memorization and retrieval processes of modern Hopfield models. While $\mathcal{T}$ retrieves memory patterns $\{\boldsymbol{\xi}_\mu\}_{\mu \in [M]}$ based on $\mathbf{x}$ with an error tolerance ϵ, the SVR problem (3.2)

- **(Memorization:)** Fits a function $\mathcal{T}_{\text{SVR}}$ satisfying Definition 3.2, which

- **(Retrieval:)** Maps queries onto memory patterns within a component-wise error-margin $\epsilon/\sqrt{d}$.

Importantly, Theorem 3.1 enables us to derive a family of nonparametric modern Hopfield models through constructing their retrieval dynamics with various kernel functions $\Phi(\cdot)$, including Dense [Ramsauer et al., 2020], Linear [Katharopoulos et al., 2020], Multi-Head [Vaswani et al., 2017], Sparse-Structured [Zaheer et al., 2020, Beltagy et al., 2020, Child et al., 2019] and Generalized Kernelizable or PRFs (Positive Random Features) [Choromanski et al., 2021] modern Hopfield models.

In Appendix C, we present constructions of these modern Hopfield models as extensions of our framework.

3.2 Nonparametric Dense and Sparse-Structured Modern Hopfield Models

In this section, we showcase the nonparametric framework Theorem 3.1 with two special cases. First, we recover the standard dense modern Hopfield model [Ramsauer et al., 2020]. Then, we introduce the efficient *sparse-structured modern Hopfield models* with sub-quadratic complexity.

Dense Modern Hopfield Model [Ramsauer et al., 2020].

Lemma 3.1 (Nonparametric Dense Modern Hopfield Model)**.** Let $\Phi(\cdot)$ =

$\left(\phi_0^{(0)}, \phi_1^{(1)}, \ldots, \phi_{D_1}^{(1)}, \ldots, \phi_1^{(n)}, \ldots, \phi_{D_n}^{(n)}, \ldots\right)$ with, for $1 \le D' \le D_n$,

$$\phi_{D'}^{(n)} := \frac{(\sqrt{\beta} x_1)^{\ell_1} \cdots (\sqrt{\beta} x_d)^{\ell_d}}{\sum_{\mu=1}^M \langle \Phi(\boldsymbol{\xi}_\mu + \delta\boldsymbol{\xi}_\mu), \Phi(\mathbf{x}) \rangle \cdot \sqrt{\ell_1! \cdots \ell_d!}}, \tag{3.5}$$

where $\ell_1 + \cdots + \ell_d = n$, and $D_n := \binom{d+n-1}{n}$. By Theorem 3.1, fitting $\mathcal{T}_{\text{SVR}}$ on $\mathcal{D}$ following (3.2) gives

$$\mathcal{T}_{\text{Dense}}(\mathbf{x}) = \boldsymbol{\Xi} \operatorname{Softmax}\left(\beta \boldsymbol{\Xi}_\delta^\top \mathbf{x}\right) \in \mathbb{R}^d, \tag{3.6}$$

where $\boldsymbol{\Xi}_\delta := [\boldsymbol{\xi}_1 + \delta\boldsymbol{\xi}_1, \cdots, \boldsymbol{\xi}_M + \delta\boldsymbol{\xi}_M] \in \mathbb{R}^{d \times M}$ denotes the contaminated memory patterns.

Proof Sketch. We first select Φ to be the Taylor expansion of the $\exp$ function via the homogeneous infinite polynomial kernel [Chen et al., 2005]. By solving the optimization problem (3.2), we arrive a retrieval dynamics resembling (2.3). See Appendix B.2 for a detailed proof. □

Remark 3.6 (*Hetero-* v.s. *Auto-*Associative Memory.)**.** So far, we derive a nonparametric framework for hetero-associative modern Hopfield models, differentiating $\mathbf{x}$ and $\mathbf{y}$ by incorporating inherent noise $\delta\boldsymbol{\xi}$ into $\mathcal{D}$. If we eliminate noises $\{\delta\boldsymbol{\xi}_\mu\}_{\mu \in [M]}$ from the training memory patterns, (3.6) reduces to that of the standard *auto-associative* dense modern Hopfield model, as shown in (2.3).

With Remark 3.6, Lemma 3.1 facilitates the replication of known results from the standard dense modern Hopfield model [Ramsauer et al., 2020]. The recovery of dense modern Hopfield model provides a sanity check for our nonparametric framework.

Sparse-Structured Modern Hopfield Models. Next, we present a set of efficient modern Hopfield models with sparse-structured patterns via the following mask.

Definition 3.3 (Sparse-Structured Mask)**.** Let $\mathcal{M} := \{\mathcal{M}(1), \ldots, \mathcal{M}(k)\} \subseteq \{1, \ldots, M\}$ be the reduced support set for $\mathcal{T}_{\text{SVR}}$ of size $k \le M$. Then, for $\mu \in [M]$, the optimization problem in (3.2) reduces to

$$\operatorname*{Min}_{\mathbf{W}, \boldsymbol{\eta}, \widetilde{\boldsymbol{\eta}}} \frac{1}{2} \|\mathbf{W}\|^2 + C \sum_{\mu \in \mathcal{M}} \langle \mathbb{1}, (\boldsymbol{\eta}_\mu + \widetilde{\boldsymbol{\eta}}_\mu) \rangle \tag{3.7}$$

subject to

$$
\begin{cases}
-(\epsilon'\mathbb{1} + \widetilde{\boldsymbol{\eta}}_\mu) \le \boldsymbol{\xi}_\mu - \langle \mathbf{W}, \Phi(\boldsymbol{\xi}_\mu + \delta\boldsymbol{\xi}_\mu) \rangle \le \epsilon'\mathbb{1} + \boldsymbol{\eta}_\mu \\
\epsilon'\mathbb{1} + \boldsymbol{\eta}_\mu \le \epsilon\mathbb{1}/\sqrt{d} \\
\boldsymbol{\eta}_\mu \ge 0, \widetilde{\boldsymbol{\eta}}_\mu \ge 0, \forall \mu \in \mathcal{M}.
\end{cases}
$$

With Definition 3.3, we obtain the following sparse-structured retrieval dynamics (and thereby its corresponding Hopfield model(s)) by fitting $\mathcal{T}_{\text{SVR}}$ on $\mathcal{D}$ masked by $\mathcal{M}$.

Theorem 3.2 (Sparse-Structured Modern Hopfield Models). Let $\Phi(\cdot) = (\phi_0^{(0)}, \phi_1^{(1)}, \ldots, \phi_{D_1}^{(1)}, \ldots, \phi_1^{(n)}, \ldots, \phi_{D_n}^{(n)}, \ldots)$ with, for $1 \le D' \le D_n$,

$$
\phi_{D'}^{(n)} := \frac{(\sqrt{\beta}x_1)^{\ell_1} \cdots (\sqrt{\beta}x_d)^{\ell_d}}{\sum_{\mu=1}^{M} \langle \Phi(\boldsymbol{\xi}_\mu + \delta\boldsymbol{\xi}_\mu), \Phi(\mathbf{x}) \rangle \cdot \sqrt{\ell_1! \cdots \ell_d!}}, \tag{3.8}
$$

where $\ell_1 + \cdots + \ell_d = n$, and $D_n := \binom{d+n-1}{n}$. By Theorem 3.1, fitting $\mathcal{T}_{\text{SVR}}$ on $\mathcal{D}$ masked by $\mathcal{M}$ following (3.7) gives

$$
\mathcal{T}_{\text{Sparse}}(\mathbf{x}) = \sum_{\mu \in \mathcal{M}} \underbrace{\left[\text{Softmax}\left(\beta \boldsymbol{\Xi}_\delta^\mathsf{T} \mathbf{x}\right)\right]_\mu}_{\in \mathbb{R}} \boldsymbol{\xi}_\mu \in \mathbb{R}^d, \tag{3.9}
$$

where $\boldsymbol{\Xi}_\delta := [\boldsymbol{\xi}_1 + \delta\boldsymbol{\xi}_1, \cdots, \boldsymbol{\xi}_M + \delta\boldsymbol{\xi}_M] \in \mathbb{R}^{d \times M}$ denotes the contaminated memory patterns.

Proof. See Appendix B.3 for a detailed proof. $\qquad\square$

We emphasize that (3.9) is in fact generic and is able to describe many sparse-structured modern Hopfield models with various support set. Importantly, it allows us to construct efficient variants with sub-quadratic complexity, and hence fills the void in the literature regarding efficient modern Hopfield models, as discussed in [Hu et al., 2023].

We present three efficient variants based on (3.9) below. To analyze efficiency for long query sequences[2], we first generalize (3.9) from a single query $\mathbf{x}$ to a sequence of L query denoted by $\mathbf{X} = [\mathbf{x}_1, \ldots, \mathbf{x}_L]$. Let the binary matrix $\mathbb{I}_\mathcal{M}$ be the corresponding sparse-sturcted mask.

Random Masked Modern Hopfield Model with $\mathcal{O}(kL)$ Complexity. By setting $\mathcal{M}$ to randomly mask $(M-k)$ entries, we obtain an efficient modern Hopfield model with a sub-quadratic $\mathcal{O}(kL)$ complexity. This model connects to the random attention of BigBird [Zaheer et al., 2020].

---

[2]Considering long query sequences is crucial, as they contribute to inefficiency (see [Hu et al., 2023, Section C.2]).

Efficient Modern Hopfield Model with $\mathcal{O}(L\sqrt{L})$ Complexity. By setting $\mathcal{M}$ for each query in a way that $\mathbb{I}_\mathcal{M}$ reproduces the sliding window pattern of window size $\sqrt{L}$, we obtain an efficient modern Hopfield model with a sub-quadratic $\mathcal{O}(L\sqrt{L})$ complexity. This model connects to the Longformer attention [Beltagy et al., 2020] by design.

Top-K Modern Hopfield Model. Let the sequence $\{p_\mu\}_{\mu\in[M]}$ be the inner products of memories $\{\boldsymbol{\xi}_\mu\}_{\mu\in[M]}$ and query $\mathbf{x}$:

$$p_\mu = \langle \mathbf{x}, \boldsymbol{\xi}_\mu \rangle \tag{3.10}$$

and let $p^\star$ be the K-th largest element in $\{p_\mu\}_{\mu\in[M]}$. Then we obtain a sparse-structured mask $\mathcal{M}$ such that

$$\begin{cases} \mu \in \mathcal{M}, \text{ if } p_\mu \geq p^\star \\ \mu \notin \mathcal{M}, \text{ if } p_\mu < p^\star. \end{cases} \tag{3.11}$$

With (3.11), we arrive a top-K modern Hopfield model with quadratic complexity, i.e., inefficient. This model connects to the top-K attention [Gupta et al., 2021] by design.

Remark 3.7 (Time Complexity of Modern Hopfield Models and Attention Mechanism)**.** The time complexity of modern Hopfield models and Hopfield layers is given by:

- Time complexity of modern Hopfield model: $\mathcal{O}(Md^2)$

- When used as cross-attention (Hopfield layer) with length-L (query) and length-M (memory) input sequences: $\mathcal{O}(LMd^2)$

- When used as self-attention with length-L input sequence (set $M = L$): $\mathcal{O}(n^2d^2)$

Our efficient modern Hopfield models achieve high efficiency through two means: a sparse-structured mask and various choices of the kernel Φ. The sparse-structured mask, with a support set size of $k \leq M$, reduces the complexity from $\mathcal{O}(Md^2)$ to $\mathcal{O}(kd^2)$. Additionally, different choices of kernel, such as the linear kernel and positive random kernel discussed in Appendix C, lead to efficient implementations.

Next, we provide analytic characterizations of how sparsity affects the sparse-structured models defined in (3.9).

4 Theoretical Analysis of Sparse-Structured Modern Hopfield Models

In this section, our theoretical analysis on sparse modern Hopfield models[3] consists of the following two aspects:

1. Derive the sparsity-dependent retrieval error bound of sparse modern Hopfield model and prove its rapid convergence property compared with its dense counterpart.

2. Characterize the fundamental limit of memory capacity of the sparse-structured modern Hopfield models.

As a reminder, we adopt Definition 3.2 for memory storage and retrieval. Additionally, we recall the following definition regarding the separation between memory patterns.

Definition 4.1 (Separation of Patterns). The separation of a memory pattern $\boldsymbol{\xi}_\mu$ from all other memory patterns Ξ is defined as its minimal inner product difference to any other patterns: $\Delta_\mu :=$ $\mathrm{Min}_{\nu,\nu\neq\mu}\left[\langle\boldsymbol{\xi}_\mu,\boldsymbol{\xi}_\mu\rangle - \langle\boldsymbol{\xi}_\mu,\boldsymbol{\xi}_\nu\rangle\right]$.

4.1 Memory Retrieval: Error Bounds & Convergence

Memory Retrieval Error Bounds. To analyze the accuracy of memory retrieval, we derive the upper bound on retrieval error of the sparse-structured models.

Theorem 4.1 (Sparsity-Dependent Retrieval Error). Let $\mathcal{T}_{\mathrm{Sparse}}$ be the sparse-structured retrieval dynamics (3.9). For query $\mathbf{x} \in \mathcal{S}_\mu$, it holds

$$\|\mathcal{T}_{\mathrm{Sparse}}(\mathbf{x}) - \boldsymbol{\xi}_\mu\| \leq \tag{4.1}$$
$$m(M + k - 2)\exp\left\{-\beta\left(\langle\boldsymbol{\xi}_\mu,\mathbf{x}\rangle - \underset{\nu\in[M],\nu\neq\mu}{\mathrm{Max}}\langle\boldsymbol{\xi}_\mu,\boldsymbol{\xi}_\nu\rangle\right)\right\},$$

for all $\mu \in \mathcal{M}$, where $k := |\mathcal{M}| \in [M]$ denotes the size of the support set $\mathcal{M}$, and $m = \mathrm{Max}_\mu \|\boldsymbol{\xi}_\mu\|$.

Proof. See Appendix B.4 for a detailed proof. □

Interestingly, the retrieval error bound in Theorem 4.1 is sparsity-dependent, which is governed by the size of the support set $\mathcal{M}$, i.e. sparsity dimension $k := |\mathcal{M}|$.

---

[3]We use plural "models" as $\mathcal{M}$ in (3.9) is a generic expression for many models with different sparse patterns.

Remark 4.1 (Comparing with the Sparse Modern Hopfield Model [Hu et al., 2023]). Compared to the retrieval error bound in [Hu et al., 2023], which lacks explicit dependence on its input (data)-dependent sparsity, the sparsity (size of $\mathcal{M}$) here is pre-specified. When there are fewer elements in the sparse-structured mask, i.e., when k is small, the retrieval error bound is tighter, and vice versa.

Remark 4.2 (Noise Robustness). By Theorem 4.1, in cases involving contaminated query or memory, i.e. $\widetilde{\mathbf{x}} = \mathbf{x} + \boldsymbol{\delta}\mathbf{x}$ (noise in query) or $\widetilde{\boldsymbol{\xi}} = \boldsymbol{\xi} + \boldsymbol{\delta}\boldsymbol{\xi}$ (noise in memory), the impact of noise on the sparse retrieval error (4.1) is less than that its impact on the dense counterpart due to the smaller coefficient $(M + k - 2)$.

Corollary 4.1.1. Let $\mathcal{T}_{\text{Dense}}$ and $\mathcal{T}_{\text{Sparse}}$ be the dense (3.9) and sparse-structured (3.9) retrieval dynamics, respectively. For any query pattern $\mathbf{x} \in \mathcal{S}_\mu$ and $\mu \in \mathcal{M}$, it holds

$$\|\mathcal{T}_{\text{Sparse}}(\mathbf{x}) - \boldsymbol{\xi}_\mu\| \leq \|\mathcal{T}_{\text{Dense}}(\mathbf{x}) - \boldsymbol{\xi}_\mu\|. \tag{4.2}$$

Proof. See Appendix B.5 for a detailed proof. □

Computationally, Corollary 4.1.1 suggests that $\mathcal{T}_{\text{Sparse}}$ necessitates fewer iterations to reach fixed points compared to $\mathcal{T}_{\text{Dense}}$, given the same error tolerance level. In other words, $\mathcal{T}_{\text{Sparse}}$ retrieves stored memory patterns faster than $\mathcal{T}_{\text{Dense}}$.

Remark 4.3 (Multiple-Update). Another important implication of Corollary 4.1.1 is that $\mathcal{T}_{\text{Sparse}}$ exhibits similar multiple-update functionality to existing models [Hu et al., 2023, Wu et al., 2024b, Ramsauer et al., 2020].

To bridge to deep learning methodologies, we show that $\mathcal{T}_{\text{Sparse}}$ retrieves memory patterns with high accuracy after a single activation in the following corollary, akin to [Hu et al., 2023, Wu et al., 2024b, Ramsauer et al., 2020].

Corollary 4.1.2 (One-Step Retrieval with High Accuracy). For any query $\mathbf{x} \in S_\mu$ and $\mu \in \mathcal{M}$, $\mathcal{T}_{\text{Sparse}}$ retrieve the memory pattern $\boldsymbol{\xi}_\mu$ with retrieval error ϵ exponentially suppressed by Δ_μ.

Proof. See Appendix B.5 for a detailed proof. □

Corollary 4.1.2 indicates that, with sufficiently large Δ_μ, $\mathcal{T}_{\text{Sparse}}$ retrieves memory patterns in a single *iteration*, allowing the integration of sparse-structured modern Hopfield models into deep learning architectures similarly to [Schimunek et al., 2023, Hoover et al., 2023, Seidl et al., 2022, Fürst et al., 2022, Paischer et al., 2022].

17

Fixed Point Convergence. By design, the retrieval dynamics constructed via Lemma 3.1 satisfy (T2). We now verify this adherence as a sanity check. Interestingly, while previous studies [Hu et al., 2023, Wu et al., 2024b, Ramsauer et al., 2020] rely on the detailed energy functions to show the convergence properties of modern Hopfield models, we prove them for sparse-structured modern Hopfield models even without knowing E in the next lemma.

Lemma 4.1 (Fixed Point Convergence). *Let* $\mathcal{T}_{\text{Sparse}}$ *be the sparse-structured retrieval dynamics (3.9). For all* $\mu \in \mathcal{M}$, *the query* $\mathbf{x} \in S_\mu$ *converges to a fixed point if it is iteratively applied by* $\mathcal{T}_{\text{Sparse}}$.

Proof. See Appendix B.6 for a detailed proof. □

Lemma 4.1 affirms that $\mathcal{T}_{\text{Sparse}}$ in (3.9) satisfies (T2).

4.2 Memory Capacity

To characterize the fundamental limit of memory capacity, we ask the following two questions for sparse-structured modern Hopfield models following [Hu et al., 2023]:

(A) What is the necessary condition for a pattern $\boldsymbol{\xi}_\mu$ being considered well-stored, and correctly retrieved?

(B) What is the expected number of memory patterns such that the above condition is satisfied?

Well-Separation Condition. To address (A), we identify the necessary condition for a pattern being well-stored and retrieved by the sparse-structured modern Hopfield models: the well-separation condition.

Theorem 4.2 (Well-Separation Condition). *Following* Definition 3.2, *for* $\mu \in \mathcal{M}$, *suppose every memory pattern* $\{\boldsymbol{\xi}_\mu\}_{\mu \in \mathcal{M}}$ *is enclosed by a sphere* $\mathcal{S}_\mu := \{\mathbf{x} \mid \|\mathbf{x} - \boldsymbol{\xi}_\mu\| \leq R\}$, *with finite radius* $R := \frac{1}{2} \text{Min}_{\mu,\nu \in \mathcal{M}; \mu \neq \nu} \|\boldsymbol{\xi}_\mu - \boldsymbol{\xi}_\nu\|$. *Then, the retrieved dynamics* $\mathcal{T}_{\text{Sparse}}$ *maps* $\mathcal{S}_\mu$ *to itself if*

1. *The starting point* $\mathbf{x}$ *is inside* $\mathcal{S}_\mu$: $\mathbf{x} \in \mathcal{S}_\mu$.
2. *The* well-separation *condition:*

$$\Delta_\mu \geq \frac{1}{\beta} \ln\left(\frac{(M+k-2)m}{R}\right) + 2mR. \tag{4.3}$$

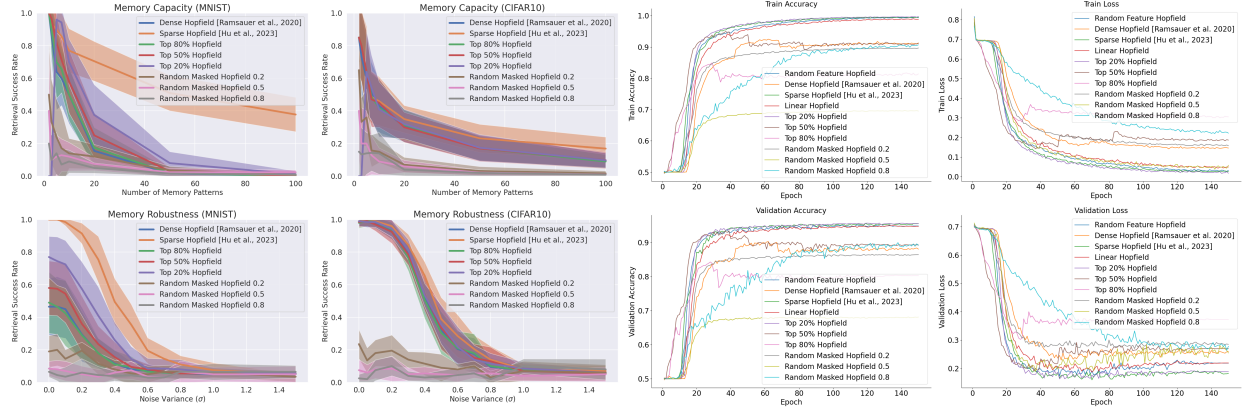*Proof.* See Appendix B.7 for a detailed proof. □

18

Figure 2: **Overview of Appendix E: Numerical Justifications for Theoretical Results.** (**Upper Left**): Memory Capacity measured by successful retrieval rates from half-masked queries (Lemma 4.2). (**Bottom Left**): Memory Robustness measured by success retrieval rates from noisy queries with different scales of Gaussian noise (Remark 4.2). For all Hopfield models, we set $\beta = .01/0.1$ (for MNIST/CIFAR10) for better visualizations. A query pattern is considered correctly retrieved if its sum-of-square similarity error is below a set threshold. For both datasets, we set the error thresholds to be 20%. Plotted are the means and standard deviations of 10 runs. We see that Top-K Hopfield shows similar exponential capacity as Dense [Ramsauer et al., 2020] and Sparse Hopfield [Hu et al., 2023]. Note that the Random Masked Hopfield models perform poorly. This is because they violate the $\mu \in \mathcal{M}$ assumption in Theorem 3.2, as the random mask might inadvertently mask out the correct pattern in the memory set. (**Upper Right**): Training loss and accuracy curve of different Hopfield models on MNIST multiple instance learning task (Theorem 4.1). (**Bottom Right**): Validation loss and accuracy curve of different Hopfield models on MNIST multiple instance learning task (Theorem 4.1). We train all the model with 150 epochs with cosine annealing learning rate decay. Plotted are the means over 10 runs. We observe that with Sparse Hopfield having the highest validation accuracy, Random feature Hopfield also shows competitive performance with faster convergence speed. On the other hand, Top 20% Hopfield also converges fast with almost no performance drop. More experimental details can be found in Appendix E.

Intuitively, the well-separation condition establishes a threshold that ensures any pattern $\{\boldsymbol{\xi}_\mu\}_{\mu \in \mathcal{M}}$ is distinguishable from all others, enabling patterns to be well-stored at a fixed point of $\mathcal{T}_{\text{Sparse}}$ and retrieved with R precision by $\mathcal{T}_{\text{Sparse}}$. Notably, Theorem 4.2 reveals that the lower bound on Δ_μ diminishes as k decreases. Consequently, as $\mathcal{M}$ becomes sparser, satisfying the well-separation condition becomes easier, facilitating the storage of patterns and leading to a larger memory capacity lower bound for sparse-structured modern Hopfield models.

Memory Capacity. To address (B), we derive the lower bound for the maximum number of memory patterns that are well-stored and retrievable according to Theorem 4.2:

Lemma 4.2 (Modified from [Hu et al., 2023]). Define the probability of storing and retrieving a memory pattern as $1 - p$. Memory capacity, the maximum number of patterns randomly sampled from a sphere with radius m that the sparse modern Hopfield models can store and retrieve, has an lower bound: $M_{\text{Sparse}} \geq \sqrt{p} C^{\frac{d-1}{4}}$, where C is the solution for the identity $C = {}^{b}/{W_0(\exp\{a+\ln b\})}$ with the principal branch of Lambert W function, $a := \left({}^{4}/{d-1}\right)\left(\ln\left[{}^{m(\sqrt{p}+k-1)}/{R}\right] + 1\right)$ and $b := {}^{4m^2\beta}/{5(d-1)}$.

Proof. See Appendix B.8 for a detailed proof. □

Remark 4.4. Theorem 4.2 gives a memory capacity exponential in the pattern size d (maximum allowed value k). Since $k \leq M$, the scaling behavior of sparse-structured modern Hopfield models is similar to that of [Ramsauer et al., 2020, Hu et al., 2023]. This result mirrors findings in [Wu et al., 2024b, Hu et al., 2023, Ramsauer et al., 2020].

5 Conclusion and Discussion

We introduce a nonparametric framework for modern Hopfield models. We use two examples to validate our framework: the original dense & the sparse-structured modern Hopfield models. With Lemma 3.1, we replicate the known results of the original modern Hopfield model [Ramsauer et al., 2020]. With Theorem 3.2, we introduce the efficient sparse-structured Hopfield models with robust theoretical properties: tighter retrieval error bound (Corollary 4.1.1 & Corollary 4.1.2), stronger noise robustness (Remark 4.2) and exponential-in-d capacity (Theorem 4.2 & Lemma 4.2).

Comparing with Existing Works. Our framework complements existing works [Hu et al., 2023, Wu et al., 2024b, Martins et al., 2023] by filling the efficiency gaps and connecting to various attentions in the following. Notably, when the size of the support set $k = M$, the results of Theorem 4.1, Theorem 4.2 and Lemma 4.2 reduce to those of the dense modern Hopfield model in [Ramsauer et al., 2020].

Extensions. In Appendix C, we present a family of modern Hopfield models connecting to many other existing attention mechanisms, including Linear [Katharopoulos et al., 2020], Multi-Head [Vaswani et al., 2017], and Generalized Kernelizable or PRFs (Positive Random Features) [Choromanski et al., 2021] modern Hopfield models.

Hopfield Layers and Numerical Experiments. In line with [Hu et al., 2023, Wu et al., 2024b, Ramsauer et al., 2020], we introduce deep learning layers as competitive attention alternatives with memory-enhanced functionalities, corresponding to our nonparametric modern Hopfield

models (sparse-structured and above extensions) in Appendix D and verify them numerically in Appendix E.

Accuracy-Efficiency Tradeoff. For learning tasks, we do not expect generally superior performance from efficient models. Ultimately, there is the provably accuracy-efficiency tradeoff [Keles et al., 2023, Deng et al., 2023] based on complexity analysis of matrix multiplication (hence, this result is transferable to modern Hopfield models [Hu et al., 2024b]). Therefore this work only provides a theoretical framework supporting the derivation of efficient variants of modern Hopfield model, with no strictly superior performance guarantee. However, we do observe that, in many cases, linear and random features modern Hopfield models deliver acceptable results.

Limitations and Future Work. A notable limitation of this work is the absence of theoretical analysis for the extensions discussed in Appendix C. We leave them for future works.

Boarder Impact

This is a theoretical work. We expect no negative social impacts. As discussed in introduction and related works, this work aims to shed some light on the foundations of large Hopfield-based foundation models.

Acknowledgments

Appendix

A   Table of Notations

Table 1: Mathematical Notations and Symbols

Symbol	Description
$\mathbf{a}[i]$	The i-th component of vector $\mathbf{a}$
$\langle \mathbf{a}, \mathbf{b} \rangle$	Inner product for vectors $\mathbf{a}, \mathbf{b} \in \mathbb{R}^d$
$[I]$	Index set $\{1, \cdots, I\}$, where $I \in \mathbb{N}^+$
$\|\cdot\|$	Spectral norm, equivalent to the l_2-norm when applied to a vector
d	Dimension of patterns
M	Number of stored memory patterns
β	Scaling factor of the energy function controlling the learning dynamics. We set $\beta = 1/\sqrt{d}$ in practice
$\mathbf{x}$	State/configuration/query pattern in $\mathbb{R}^d$
$\mathbf{x}^\star$	Stationary points of the Hopfield energy function
$\boldsymbol{\xi}$	Memory patterns (keys) in $\mathbb{R}^d$
$\delta\boldsymbol{\xi}$	Noises in memory patterns in $\mathbb{R}^d$
$\mathcal{D}$	Training data set $\{(\boldsymbol{\xi}_\mu + \delta\boldsymbol{\xi}_\mu, \boldsymbol{\xi}_\mu)\}_{\mu \in [M]}$
Ξ	Shorthand for M stored memory (key) patterns $\{\boldsymbol{\xi}_\mu\}_{\mu \in [M]}$ in $\mathbb{R}^{d \times M}$
Ξ_δ	Shorthand for M contaminated memory (key) patterns $\{\delta\boldsymbol{\xi}_\mu\}_{\mu \in [M]}$ in $\mathbb{R}^{d \times M}$
$\Xi^\mathsf{T}\mathbf{x}$	M-dimensional overlap vector $(\langle \boldsymbol{\xi}_1, \mathbf{x} \rangle, \cdots, \langle \boldsymbol{\xi}_\mu, \mathbf{x} \rangle, \cdots, \langle \boldsymbol{\xi}_M, \mathbf{x} \rangle)$ in $\mathbb{R}^M$
$\Phi(\cdot)$	Kernelized feature mapping $\Phi(\cdot) : \mathbb{R}^d \to D_\phi$
ϕ	Element in the $\Phi(\cdot) = (\phi_0^{(0)}, \phi_1^{(1)}, \ldots, \phi_{D_1}^{(1)}, \ldots, \phi_1^{(n)}, \ldots, \phi_{D_n}^{(n)}, \ldots)$
D_Φ	Dimension of the kernel space, i.e., dimension of output of $\Phi(\cdot)$
$h(\cdot)$	Normalization mapping in the regression model defined by (3.1)
$\mathbf{W}$	Weighted matrix in the regression model defined by (3.1) in $\mathbb{R}^{d \times D_\Phi}$
$\mathbf{w}_i$	i-th row of the weighted matrix $\mathbf{W}$ in $\mathbb{R}^{D_\Phi}$
$\mathcal{K}(\cdot, \cdot)$	Kernel function takes the inner product form $\mathcal{K}(\cdot, \cdot) = \langle \Phi(\cdot), \Phi(\cdot) \rangle$ in $\mathcal{K} : \mathbb{R}^{D_\Phi} \times \mathbb{R}^{D_\Phi} \to \mathbb{R}_+$
ϵ'	Component-wise term error margin in the support vector regression problem
$\boldsymbol{\eta}, \widetilde{\boldsymbol{\eta}}$	Slack variables in the support vector regression
C	Penalized coefficient of the support vector regression
$\mathcal{L}$	Lagrangian corresponding to (3.2)
$\boldsymbol{\alpha}, \widetilde{\boldsymbol{\alpha}}, \boldsymbol{\lambda}, \widetilde{\boldsymbol{\lambda}}$	Dual variables in the Lagrangian $\mathcal{L}$
$\mathcal{M}$	Reduced support set for $\mathcal{T}_{\text{SVR}}$ $\mathcal{M} := \{\mathcal{M}(1), \ldots, \mathcal{M}(k)\} \subseteq \{1, \ldots, M\}$
$\mathbb{1}_{\mathcal{M}(\mu)}$	Indicator function corresponding to $\mathcal{M}$, where $\mathbb{1}_{\mathcal{M}(\mu)} = 1$ for $\mu \in \mathcal{M}$ and $\mathbb{1}_{\mathcal{M}(\mu)} = 0$ for $\mu \notin \mathcal{M}$
k	Size of the support set $\mathcal{M}$, defined as $k := |\mathcal{M}|$
m	Largest norm of memory patterns, denoted as $m := \text{Max}_{\mu \in [M]} \|\boldsymbol{\xi}_\mu\|$
R	Minimal Euclidean distance across all possible pairs of memory patterns, denoted as $R := \frac{1}{2} \text{Min}_{\mu, \nu \in [M]} \|\boldsymbol{\xi}_\mu - \boldsymbol{\xi}_\nu\|$
S_μ	Sphere centered at memory pattern $\boldsymbol{\xi}_\mu$ with finite radius R
$\mathbf{x}_\mu^\star$	Fixed point of $\mathcal{T}$ covered by S_μ, i.e., $\mathbf{x}_\mu^\star \in S_\mu$
Δ_μ	Separation of a memory pattern $\boldsymbol{\xi}_\mu$ from all other memory patterns Ξ, defined in (4.1)
$\widetilde{\Delta}_\mu$	Separation of $\boldsymbol{\xi}_\mu$ at a given $\mathbf{x}$ from all memory patterns Ξ, defined in (4.1)

B Proofs of Main Text

B.1 Theorem 3.1

Proof of Theorem 3.1. The Lagrangian of convex optimization problem defined in (3.2) is

$$
\begin{aligned}
\mathcal{L} := &\frac{1}{2} \sum_{i=1}^{d} \|\mathbf{w}_i\|^2 + C \sum_{\mu=1}^{M} \sum_{i=1}^{d} (\boldsymbol{\lambda}_\mu[i]\boldsymbol{\eta}_\mu[i] + \widetilde{\boldsymbol{\lambda}}_\mu[i]\widetilde{\boldsymbol{\eta}}_\mu[i]) \\
&- \sum_{\mu=1}^{M} \sum_{i=1}^{d} \boldsymbol{\alpha}_\mu[i] \left(\epsilon' + \boldsymbol{\eta}_\mu[i] - \boldsymbol{\xi}_\mu[i] + \langle \mathbf{w}_i, \Phi(\boldsymbol{\xi}_\mu + \delta\boldsymbol{\xi}_\mu) \rangle \right) \\
&- \sum_{\mu=1}^{M} \sum_{i=1}^{d} \widetilde{\boldsymbol{\alpha}}_\mu[i] \left(\epsilon' + \widetilde{\boldsymbol{\eta}}_\mu[i] - \langle \mathbf{w}_i, \Phi(\boldsymbol{\xi}_\mu + \delta\boldsymbol{\xi}_\mu) \rangle + \boldsymbol{\xi}_\mu[i] \right),
\end{aligned}
\tag{B.1}
$$

where $\boldsymbol{\lambda}_\mu[i]$, $\widetilde{\boldsymbol{\lambda}}_\mu[i]$, $\boldsymbol{\alpha}_\mu[i]$ and $\widetilde{\boldsymbol{\alpha}}_\mu[i]$ are Lagrange multipliers. Next, we solve stationary condition with respect to $\mathbf{w}_i, \boldsymbol{\eta}_\mu[i]$ and $\widetilde{\boldsymbol{\eta}}_\mu[i]$ from above Lagrangian and derive corresponding optimal solution. The Lagrangian in (B.1) admits a stationary solution, which is given by:

$$
\begin{cases}
\mathbf{w}_i - \sum_{\mu=1}^{M} (\boldsymbol{\alpha}_\mu[i] - \widetilde{\boldsymbol{\alpha}}_\mu[i]) \Phi(\boldsymbol{\xi}_\mu + \delta\boldsymbol{\xi}_\mu) = 0, \\
C - \boldsymbol{\lambda}_\mu[i] - \boldsymbol{\alpha}_\mu[i] = 0, \\
C - \widetilde{\boldsymbol{\lambda}}_\mu[i] - \widetilde{\boldsymbol{\alpha}}_\mu[i] = 0.
\end{cases}
\tag{B.2}
$$

Substitute (B.2) into (3.1) to write

$$
\mathbf{x}^{\text{new}}[i] = \mathcal{T}_{\text{SVR}}(\mathbf{x})[i] := \langle \mathbf{w}_i^\star, \Phi(\mathbf{x}) \rangle,
\tag{B.3}
$$

with the learned weight matrix

$$
\mathbf{w}_i^\star := \sum_{\mu=1}^{M} \underbrace{(\boldsymbol{\alpha}_\mu[i] - \widetilde{\boldsymbol{\alpha}}_\mu[i])}_{\in \mathbb{R}} \underbrace{\Phi(\boldsymbol{\xi}_\mu + \delta\boldsymbol{\xi}_\mu)}_{\in \mathbb{R}^{D_\Phi}} \in \mathbb{R}^{D_\Phi}.
\tag{B.4}
$$

The complementary slackness condition and dual feasibility of (B.1) are given by

$$
\begin{cases}
\boldsymbol{\alpha}_\mu[i] \left(\epsilon' + \boldsymbol{\eta}_\mu[i] - \boldsymbol{\xi}_\mu[i] + \langle \mathbf{w}_i, \Phi(\boldsymbol{\xi}_\mu + \delta\boldsymbol{\xi}_\mu) \rangle \right) = 0 \\
\widetilde{\boldsymbol{\alpha}}_\mu[i] \left(\epsilon' + \widetilde{\boldsymbol{\eta}}_\mu[i] - \langle \mathbf{w}_i, \Phi(\boldsymbol{\xi}_\mu + \delta\boldsymbol{\xi}_\mu) \rangle + \boldsymbol{\xi}_\mu[i] \right) = 0 \\
\boldsymbol{\alpha}_\mu[i], \widetilde{\boldsymbol{\alpha}}_\mu[i], \boldsymbol{\lambda}_\mu[i], \widetilde{\boldsymbol{\lambda}}_\mu[i] \geq 0,
\end{cases}
\tag{B.5}
$$

for all $\mu \in [M]$ and $i \in [d]$. $\hfill \square$

B.2   Lemma 3.1

To simplify our proofs, we define

$$\Phi(\mathbf{x}) := \frac{\overline{\Phi}(\mathbf{x})}{h(\mathbf{x})}, \tag{B.6}$$

where $h(\cdot) : \mathbb{R}^d \to \mathbb{R}$ is some normalization function for later convenience.

To prove Lemma 3.1, we introduce the following three auxiliary lemmas.

Lemma B.1. Let $\boldsymbol{\alpha}_\mu[i] \geq 0$, $\widetilde{\boldsymbol{\alpha}}_\mu[i] \geq 0$ be a solution to (B.2) with KKT conditions (B.5). Then $\boldsymbol{\alpha}_\mu[i] - \widetilde{\boldsymbol{\alpha}}_\mu[i]$ has the following bounds

$$-C \leq \boldsymbol{\alpha}_\mu[i] - \widetilde{\boldsymbol{\alpha}}_\mu[i] \leq C, \forall \mu \in [M], i \in [d] \tag{B.7}$$

Proof. We prove this lemma by contradiction. Recall that for each fixed values of μ and i

$$\boldsymbol{\alpha}_\mu[i] \geq 0, \widetilde{\boldsymbol{\alpha}}_\mu[i] \geq 0. \tag{B.8}$$

Firstly, we assume $\boldsymbol{\alpha}_\mu[i], \widetilde{\boldsymbol{\alpha}}_\mu[i] \in \mathbb{R}_+$ (*non-zero*), for all $\mu \in [M]$ and $i \in [d]$. Recall complementary slackness conditions from (B.5)

$$\begin{cases} \epsilon' + \boldsymbol{\eta}_\mu[i] - \boldsymbol{\xi}_\mu[i] + \langle \mathbf{w}_i, \Phi(\boldsymbol{\xi}_\mu + \delta\boldsymbol{\xi}_\mu) \rangle = 0 \\ \epsilon' + \widetilde{\boldsymbol{\eta}}_\mu[i] - \langle \mathbf{w}_i, \Phi(\boldsymbol{\xi}_\mu + \delta\boldsymbol{\xi}_\mu) \rangle + \boldsymbol{\xi}_\mu[i] = 0. \end{cases} \tag{B.9}$$

Combine above two equations to write

$$\boldsymbol{\eta}_\mu[i] + \widetilde{\boldsymbol{\eta}}_\mu[i] = -2\epsilon' \leq 0. \tag{B.10}$$

Since the component-wise error $\epsilon' \geq 0$, we have $\boldsymbol{\eta}_\mu[i] + \widetilde{\boldsymbol{\eta}}_\mu[i] \leq 0$. This conclusion contradicts the assumption of the non-negative condition on slack variables $\boldsymbol{\eta}_\mu[i], \widetilde{\boldsymbol{\eta}}_\mu[i] \geq 0$. Therefore, together with (B.2), at least one of $\boldsymbol{\alpha}_\mu[i], \widetilde{\boldsymbol{\alpha}}_\mu[i]$ must be 0, for all μ and all i. Subsequently, we have

$$0 \leq \boldsymbol{\alpha}_\mu[i] \leq C \quad \text{and} \quad 0 \leq \widetilde{\boldsymbol{\alpha}}_\mu[i] \leq C, \tag{B.11}$$

which leads to

$$-C \leq \boldsymbol{\alpha}_\mu[i] - \widetilde{\boldsymbol{\alpha}}_\mu[i] \leq C. \tag{B.12}$$

$\square$

Lemma B.2 (Multinomial Expansion)**.** Given $\mathbf{x}, \mathbf{y} \in \mathbb{R}^d$. The identity

$$\frac{(\mathbf{x}^\mathsf{T}\mathbf{y})^n}{n!} = \sum_{\ell_1 + \cdots + \ell_d = n} \left(\frac{x_1^{\ell_1} \cdots x_d^{\ell_d}}{\sqrt{\ell_1! \cdots \ell_d!}} \right) \left(\frac{y_1^{\ell_1} \cdots y_d^{\ell_d}}{\sqrt{\ell_1! \cdots \ell_d!}} \right)$$

holds for all $n \in \mathbb{N}$.

Proof.

$$\begin{aligned}
\frac{(\mathbf{x}^\mathsf{T}\mathbf{y})^n}{n!} &= \frac{1}{n!}(x_1 y_1 + \cdots + x_d y_d)^n \\
&= \frac{1}{n!}\left[(x_1 y_1)^n + \cdots + \frac{n!}{\ell_1! \cdots \ell_d!} \prod_{i=1}^{d} (x_i y_i)^{\ell_i} + \cdots + (x_d y_d)^n \right] \qquad \left(\sum_{i=1}^{d} \ell_i = n \right) \\
&= \sum_{\ell_1 + \cdots + \ell_d = n} \frac{1}{\ell_1! \cdots \ell_d!} \prod_{i=1}^{d} (x_i)^{\ell_i} \prod_{i=1}^{d} (y_i)^{\ell_i} \\
&= \sum_{\ell_1 + \cdots + \ell_d = n} \frac{\left(x_1^{\ell_1} \cdots x_d^{\ell_d} \right) \left(y_1^{\ell_1} \cdots y_d^{\ell_d} \right)}{\ell_1! \cdots \ell_d!} \\
&= \sum_{\ell_1 + \cdots + \ell_d = n} \left(\frac{x_1^{\ell_1} \cdots x_d^{\ell_d}}{\sqrt{\ell_1! \cdots \ell_d!}} \right) \left(\frac{y_1^{\ell_1} \cdots y_d^{\ell_d}}{\sqrt{\ell_1! \cdots \ell_d!}} \right).
\end{aligned}$$

$\square$

Lemma B.3. Let $\mathcal{K}(\cdot, \cdot)$ be the homogeneous infinite polynomial kernel [Chen et al., 2005]:

$$\mathcal{K}(\mathbf{x}, \mathbf{y}) = \left\langle \overline{\Phi}(\mathbf{x}), \overline{\Phi}(\mathbf{y}) \right\rangle := \sum_{n=0}^{\infty} \frac{(\mathbf{x}^\mathsf{T}\mathbf{y})^n}{n!}, \tag{B.13}$$

where $\mathbf{x}, \mathbf{y} \in \mathbb{R}^d$ and Φ maps the feature vectors $\mathbf{x}$ and $\mathbf{y}$ into infinite dimensional space. Then, $\overline{\Phi}(\cdot) = (\bar{\phi}_0^{(0)}, \bar{\phi}_1^{(1)}, \ldots, \bar{\phi}_{D_1}^{(1)}, \ldots, \bar{\phi}_1^{(n)}, \ldots, \bar{\phi}_{D_n}^{(n)}, \ldots)$ has a closed form solution

$$\bar{\phi}_{D'}^{(n)} = \frac{x_1^{\ell_1} \cdots x_d^{\ell_d}}{\sqrt{\ell_1! \cdots \ell_d!}}, \tag{B.14}$$

where $\ell_1 + \cdots + \ell_d = n$, $1 \leq D' \leq D_n$ and $D_n := \binom{d+n-1}{n}$.

Proof. Applying Lemma B.2 on homogeneous infinite polynomial kernel, we have

$$\langle \overline{\Phi}(\mathbf{x}), \overline{\Phi}(\mathbf{y}) \rangle = \sum_{n=0}^{\infty} \frac{(\mathbf{x}^\mathsf{T}\mathbf{y})^n}{n!}$$

$$= \sum_{n=0}^{\infty} \sum_{\ell_1 + \cdots + \ell_d = n} \frac{1}{\ell_1! \cdots \ell_d!} \prod_{i=1}^{d} (x_i)^{\ell_i} \prod_{i=1}^{d} (y_i)^{\ell_i}$$

$$= \sum_{n=0}^{\infty} \sum_{\ell_1 + \cdots + \ell_d = n} \frac{\left(x_1^{\ell_1} \cdots x_d^{\ell_d}\right) \left(y_1^{\ell_1} \cdots y_d^{\ell_d}\right)}{\ell_1! \cdots \ell_d!}$$

$$= \sum_{n=0}^{\infty} \sum_{\ell_1 + \cdots + \ell_d = n} \left(\frac{x_1^{\ell_1} \cdots x_d^{\ell_d}}{\sqrt{\ell_1! \cdots \ell_d!}} \right) \left(\frac{y_1^{\ell_1} \cdots y_d^{\ell_d}}{\sqrt{\ell_1! \cdots \ell_d!}} \right).$$

From above, we observe that, for each fixed n, there are $\binom{d+n-1}{n}$ terms in the summation. Consequently, $\overline{\Phi}(\mathbf{x})$ has a solution

$$\overline{\Phi}(\mathbf{x}) = (\overline{\phi}_0^{(0)}, \underbrace{\overline{\phi}_1^{(1)}, \ldots, \overline{\phi}_{D_1}^{(1)}}_{\binom{d+1-1}{1} \text{ elements}}, \ldots, \underbrace{\overline{\phi}_1^{(n)}, \ldots, \overline{\phi}_{D_n}^{(n)}}_{\binom{d+n-1}{n} \text{ elements}}, \ldots), \tag{B.15}$$

where $D_n = \binom{d+n-1}{n}$ and

$$\overline{\phi}_{D'}^{(n)} = \frac{x_1^{\ell_1} \cdots x_d^{\ell_d}}{\sqrt{\ell_1! \cdots \ell_d!}} \tag{B.16}$$

for $1 \leq D' \leq D_n$ and $\ell_1 + \cdots + \ell_d = n$. $\qquad \square$

Proof of Lemma 3.1. Recall that the learned weight matrix $\mathbf{W}$ is composed of

$$\mathbf{w}_i^\star = \sum_{\mu=1}^{M} (\boldsymbol{\alpha}_\mu[i] - \widetilde{\boldsymbol{\alpha}}_\mu[i]) \frac{\overline{\Phi}(\boldsymbol{\xi}_\mu + \delta\boldsymbol{\xi}_\mu)}{h(\mathbf{x})}. \tag{B.17}$$

Substitute $\mathbf{w}^\star$ into (3.1) to write

$$\mathcal{T}_{\text{Dense}}(\mathbf{x}) = \left(\sum_{\mu=1}^{M} \frac{\alpha_\mu[1] - \widetilde{\alpha}_\mu[1]}{h(\boldsymbol{\xi}_\mu + \delta\boldsymbol{\xi}_\mu)} \frac{\langle \overline{\Phi}(\boldsymbol{\xi}_\mu + \delta\boldsymbol{\xi}_\mu), \overline{\Phi}(\mathbf{x}) \rangle}{h(\mathbf{x})}, \cdots, \sum_{\mu=1}^{M} \frac{\alpha_\mu[d] - \widetilde{\alpha}_\mu[d]}{h(\boldsymbol{\xi}_\mu + \delta\boldsymbol{\xi}_\mu)} \frac{\langle \overline{\Phi}(\boldsymbol{\xi}_\mu + \delta\boldsymbol{\xi}_\mu), \overline{\Phi}(\mathbf{x}) \rangle}{h(\mathbf{x})} \right).$$

$$\tag{B.18}$$

Let $\left(\frac{\alpha_\mu[1] - \widetilde{\alpha}_\mu[1]}{h(\boldsymbol{\xi}_\mu + \delta\boldsymbol{\xi}_\mu)}, \ldots, \frac{\alpha_\mu[d] - \widetilde{\alpha}_\mu[d]}{h(\boldsymbol{\xi}_\mu + \delta\boldsymbol{\xi}_\mu)} \right) = \boldsymbol{\xi}_\mu$ and $h(\mathbf{x}) \coloneqq \sum_{\mu=1}^{M} \left\langle \overline{\Phi}(\boldsymbol{\xi}_\nu + \delta\boldsymbol{\xi}_\nu), \overline{\Phi}(\mathbf{x}) \right\rangle$. Then $\mathcal{T}_{\text{Dense}}$ reduces to following formulation:

$$\mathcal{T}_{\text{Dense}}(\mathbf{x}) = \sum_{\mu=1}^{M} \frac{\left\langle \overline{\Phi}(\boldsymbol{\xi}_\mu + \delta\boldsymbol{\xi}_\mu), \overline{\Phi}(\mathbf{x}) \right\rangle}{\sum_{\nu=1}^{M} \left\langle \overline{\Phi}(\boldsymbol{\xi}_\nu + \delta\boldsymbol{\xi}_\nu), \overline{\Phi}(\mathbf{x}) \right\rangle} \boldsymbol{\xi}_\mu. \tag{B.19}$$

Following Lemma B.3, here we define the inner product of $\overline{\Phi}$ as a kernel $\mathcal{K} : \mathbb{R}^{D_\phi} \times \mathbb{R}^{D_\phi} \to \mathbb{R}_+$

$$\left\langle \overline{\Phi}(\mathbf{x}), \overline{\Phi}(\boldsymbol{\xi}_\mu + \delta\boldsymbol{\xi}_\mu) \right\rangle \coloneqq \mathcal{K}(\mathbf{x}, \boldsymbol{\xi}_\mu + \delta\boldsymbol{\xi}_\mu). \tag{B.20}$$

$\mathcal{T}_{\text{Dense}}$ is now given by

$$\mathcal{T}_{\text{Dense}}(\mathbf{x}) = \sum_{\mu=1}^{M} \frac{\mathcal{K}(\mathbf{x}, \boldsymbol{\xi}_\mu + \delta\boldsymbol{\xi}_\mu)}{\sum_{\nu=1}^{M} \mathcal{K}(\mathbf{x}, \boldsymbol{\xi}_\nu + \delta\boldsymbol{\xi}_\nu)} \boldsymbol{\xi}_\mu. \tag{B.21}$$

Observe that (2.3) $\mathcal{T}_{\text{Dense}}$ takes a Boltzmann form: $\exp\{\cdot\} / \sum_{\nu=1}^{M} \exp\{\cdot\}$. Recall Lemma B.3, we take

$$\overline{\phi}_{D'}^{(n)} = \frac{(\sqrt{\beta}x_1)^{\ell_1} \cdots (\sqrt{\beta}x_d)^{\ell_d}}{\sqrt{\ell_1! \cdots \ell_d!}}, \tag{B.22}$$

with the kernel

$$\mathcal{K}(\mathbf{x}, \boldsymbol{\xi}_\mu + \delta\boldsymbol{\xi}_\mu) = \sum_{n=0}^{\infty} \frac{(\langle \sqrt{\beta}\mathbf{x}, \sqrt{\beta}\boldsymbol{\xi}_\mu + \sqrt{\beta}\delta\boldsymbol{\xi}_\mu \rangle)^n}{n!}. \tag{B.23}$$

Substitute (B.23) into (B.21) to write

$$\mathcal{T}_{\text{Dense}}(\mathbf{x}) = \sum_{\mu=1}^{M} \frac{\sum_{n=0}^{\infty} \left(\langle \sqrt{\beta}\mathbf{x}, \sqrt{\beta}\boldsymbol{\xi}_\mu + \sqrt{\beta}\delta\boldsymbol{\xi}_\mu \rangle \right)^n / n!}{\sum_{\nu=1}^{M} \sum_{t=0}^{\infty} \left(\langle \sqrt{\beta}\mathbf{x}, \sqrt{\beta}\boldsymbol{\xi}_\nu + \sqrt{\beta}\delta\boldsymbol{\xi}_\nu \rangle \right)^t / t!} \boldsymbol{\xi}_\mu. \tag{B.24}$$

By Taylor's theorem, $\mathcal{T}_{\text{Dense}}$ takes the form

$$\mathcal{T}_{\text{Dense}}(\mathbf{x}) = \sum_{\mu=1}^{M} \frac{\exp\{\beta \langle \mathbf{x}, \boldsymbol{\xi}_\mu + \delta\boldsymbol{\xi}_\mu \rangle\}}{\sum_{\nu=1}^{M} \exp\{\beta \langle \mathbf{x}, \boldsymbol{\xi}_\nu + \delta\boldsymbol{\xi}_\nu \rangle\}} \boldsymbol{\xi}_\mu = \boldsymbol{\Xi} \operatorname{Softmax}\left(\beta\boldsymbol{\Xi}_\delta^{\mathsf{T}}\mathbf{x} \right), \tag{B.25}$$

where $\boldsymbol{\Xi} = (\boldsymbol{\xi}_1, \cdots, \boldsymbol{\xi}_M) \in \mathbb{R}^{d \times M}$ and $\boldsymbol{\Xi}_\delta = (\boldsymbol{\xi}_1 + \delta\boldsymbol{\xi}_1, \cdots, \boldsymbol{\xi}_M + \delta\boldsymbol{\xi}_M) \in \mathbb{R}^{d \times M}$ denote memories and noises in memories, respectively. $\qquad \square$

B.3 Theorem 3.2

Proof of Theorem 3.2. To take $\mathbf{w}^\star$ for the sparse-structured model, the partial derivatives of $\mathcal{L}$ with respect to $\mathbf{w}_i, \boldsymbol{\eta}_\mu[i]$ and $\widetilde{\boldsymbol{\eta}}_\mu[i]$ must satisfy the stationarity condition

$$\begin{cases} \mathbf{w}_i - \sum_{\mu \in \mathcal{M}} (\boldsymbol{\alpha}_\mu[i] - \widetilde{\boldsymbol{\alpha}}_\mu[i]) \, \Phi(\boldsymbol{\xi}_\mu + \delta\boldsymbol{\xi}_\mu) = 0, \\ C - \boldsymbol{\lambda}_\mu[i] - \boldsymbol{\alpha}_\mu[i] = 0, \\ C - \widetilde{\boldsymbol{\lambda}}_\mu[i] - \widetilde{\boldsymbol{\alpha}}_\mu[i] = 0. \end{cases} \tag{B.26}$$

Then, we arrive

$$\mathbf{w}_i^\star = \sum_{\mu \in \mathcal{M}} (\boldsymbol{\alpha}_\mu[i] - \widetilde{\boldsymbol{\alpha}}_\mu[i]) \frac{\overline{\Phi}(\boldsymbol{\xi}_\mu + \delta\boldsymbol{\xi}_\mu)}{h(\mathbf{x})} \tag{B.27}$$

By approach similar to Appendix B.2, we obtain the retrieval dynamics for sparse-structured modern Hopfield model:

$$\mathcal{T}_{\text{Sparse}}(\mathbf{x}) = \sum_{\mu \in \mathcal{M}} \left[\text{Softmax}\left(\beta \boldsymbol{\Xi}_\delta^\mathsf{T} \mathbf{x}\right) \right]_\mu \boldsymbol{\xi}_\mu. \tag{B.28}$$

$\square$

B.4 Theorem 4.1

Proof of Theorem 4.1. To connect $\mathcal{T}_{\text{Sparse}}$ with Δ_μ, first we derive the bound on $\|\mathcal{T}_{\text{Sparse}}(\mathbf{x}) - \boldsymbol{\xi}_\mu\|$ via [Ramsauer et al., 2020] for $\mu \in \mathcal{M}$

$$\|\mathcal{T}_{\text{Sparse}}(\mathbf{x}) - \boldsymbol{\xi}_\mu\| \le \left\| \boldsymbol{\xi}_\mu - \sum_{\nu \in \mathcal{M}} \left[\text{Softmax}\left(\beta \boldsymbol{\Xi}_\delta^\mathsf{T} \mathbf{x}\right) \right]_\nu \boldsymbol{\xi}_\nu \right\|$$

$$\le \left\| (1 - [\text{Softmax}(\beta \boldsymbol{\Xi}_\delta^\mathsf{T} \mathbf{x})]_\mu) \boldsymbol{\xi}_\mu + \sum_{\nu \in \mathcal{M}, \nu \ne \mathcal{M}} [\text{Softmax}(\beta \boldsymbol{\Xi}_\delta^\mathsf{T} \mathbf{x})]_\nu \boldsymbol{\xi}_\nu \right\| \tag{B.29}$$

$$\le \widetilde{\epsilon} \|\boldsymbol{\xi}_\mu\| + \frac{\widetilde{\epsilon}}{M - 1} \sum_{\nu \in \mathcal{M}, \nu \ne \mu} \|\boldsymbol{\xi}_\nu\| \le \widetilde{\epsilon} m + \frac{\widetilde{\epsilon}}{M - 1}(k - 1)m \tag{B.30}$$

$$\le m \frac{M + k - 2}{M - 1} \widetilde{\epsilon} \tag{B.31}$$

$$= m(M + k - 2) \exp\left\{ -\beta \left(\langle \mathbf{x}, \boldsymbol{\xi}_\mu \rangle - \max_{\nu \in [M]} \langle \mathbf{x}, \boldsymbol{\xi}_\nu \rangle \right) \right\}, \tag{B.32}$$

where $k := |\mathcal{M}|$, $m := \text{Max}_\mu \|\boldsymbol{\xi}_\mu\|$, $\widetilde{\epsilon} := (M-1)\exp\{-\beta\left(\langle \mathbf{x}, \boldsymbol{\xi}_\mu \rangle - \text{Max}_{\nu \in [M]} \langle \mathbf{x}, \boldsymbol{\xi}_\nu \rangle\right)\}$ and the inequality

$$
\left[\text{Softmax}(\beta \boldsymbol{\Xi}^\mathsf{T} \mathbf{x})\right]_\nu = \frac{\exp\{\beta\left(\langle \mathbf{x}, \boldsymbol{\xi}_\nu \rangle - \langle \mathbf{x}, \boldsymbol{\xi}_\mu \rangle\right)\}}{1 + \sum_{\nu' \neq \mu} \exp\{\beta\left(\langle \mathbf{x}, \boldsymbol{\xi}_{\nu'} \rangle - \langle \mathbf{x}, \boldsymbol{\xi}_\mu \rangle\right)\}} \leq \exp\left\{-\beta\left(\langle \mathbf{x}, \boldsymbol{\xi}_\mu \rangle - \underset{\nu \in [M]}{\text{Max}} \langle \mathbf{x}, \boldsymbol{\xi}_\nu \rangle\right)\right\},
$$

(B.33)

is used in (B.32). □

B.5 Corollary 4.1.1 and Corollary 4.1.2

Proof of Corollary 4.1.1 and Corollary 4.1.2. Since the support set of *dense* modern Hopfield model is full, i.e. $k = M$, (B.32) reduces to

$$
\|\mathcal{T}_{\text{Dense}}(\mathbf{x}) - \boldsymbol{\xi}_\mu\| \leq 2m(M-1)\exp\left\{-\beta\left(\langle \mathbf{x}, \boldsymbol{\xi}_\mu \rangle - \underset{\nu \in [M]}{\text{Max}} \langle \mathbf{x}, \boldsymbol{\xi}_\nu \rangle\right)\right\}.
$$

(B.34)

Comparing (B.32) with (B.34), we obtain

$$
\|\mathcal{T}_{\text{Sparse}}(\mathbf{x}) - \boldsymbol{\xi}_\mu\| \leq \|\mathcal{T}_{\text{Dense}}(\mathbf{x}) - \boldsymbol{\xi}_\mu\|.
$$

(B.35)

From [Ramsauer et al., 2020, Theorem 4], for any query $\mathbf{x}$, $\mathcal{T}_{\text{Dense}}$ approximately retrieves a memory pattern $\boldsymbol{\xi}_\mu$ with retrieval error ϵ exponentially suppressed by Δ_μ:

$$
\|\mathcal{T}(\mathbf{x}) - \boldsymbol{\xi}_\mu\| \leq 2m(M-1)\exp\{-\beta\left(\Delta_\mu - 2m\,\text{Max}\left[\|\mathbf{x} - \boldsymbol{\xi}_\mu\|, \|\mathbf{x} - \mathbf{x}_\mu^\star\|\right]\right)\}.
$$

(B.36)

By (B.35), $\mathcal{T}_{\text{Sparse}}$ also enjoys above retrieval error bound. Therefore, $\mathcal{T}_{\text{Sparse}}(\mathbf{x})$ retrieves a memory pattern $\boldsymbol{\xi}_\mu$ with high accuracy after a single activation with a sufficiently large Δ_μ. □

B.6 Lemma 4.1

Proof of Lemma 4.1. Recall [Hu et al., 2023, Lemma 2.2] that for initial query $\mathbf{x}_0 \in S_\mu$

$$
\lim_{t \to \infty} \|\mathbf{x}_t - \boldsymbol{\xi}_\mu\| = 0,
$$

(B.37)

where $\{\mathbf{x}_t\}_{t=0}^\infty$ is a sequence generated by $\mathcal{T}_{\text{Dense}}$ from $\mathbf{x}_0$, i.e. $\mathcal{T}_{\text{Dense}}(\mathbf{x}_t) = \mathbf{x}_{t+1}$.

Moreover, recall that for any query pattern $\mathbf{x} \in S_\mu$

$$
0 \leq \|\mathcal{T}_{\text{Sparse}}(\mathbf{x}) - \boldsymbol{\xi}_\mu\| \leq \|\mathcal{T}_{\text{Dense}}(\mathbf{x}) - \boldsymbol{\xi}_\mu\|.
$$

(B.38)

By applying squeeze theorem on (B.38) and (B.37), we have

$$\lim_{t\to\infty} \|\widetilde{\mathbf{x}}_t - \boldsymbol{\xi}_\mu\| = 0, \tag{B.39}$$

where $\{\widetilde{\mathbf{x}}_t\}_{t=0}^\infty$ is a sequence generated by $\mathcal{T}_{\text{Sparse}}$, i.e. $\mathcal{T}_{\text{Sparse}}(\widetilde{\mathbf{x}}_t) = \widetilde{\mathbf{x}}_{t+1}$.

$\square$

B.7 Theorem 4.2

Proof of 4.2. Following [Wu et al., 2024b, Hu et al., 2023], we define the separation of $\boldsymbol{\xi}_\mu$ at a given $\mathbf{x}$ from all memory patterns Ξ as

$$\widetilde{\Delta}_\mu := \underset{\nu,\nu\neq\mu}{\text{Min}} \left[\langle \mathbf{x}, \boldsymbol{\xi}_\mu \rangle - \langle \mathbf{x}, \boldsymbol{\xi}_\nu \rangle \right]. \tag{B.40}$$

Plug above into (B.32), and get

$$\|\mathcal{T}_{\text{Sparse}}(\mathbf{x}) - \boldsymbol{\xi}_\mu\| \leq m(M + k - 2)\exp\left\{-\beta\widetilde{\Delta}_\mu\right\}. \tag{B.41}$$

By Cauchy-Schwartz inequality, for all $\mu \in \mathcal{M}$,

$$|\langle \boldsymbol{\xi}_\mu, \boldsymbol{\xi}_\mu \rangle - \langle \mathbf{x}, \boldsymbol{\xi}_\mu \rangle| \leq \|\boldsymbol{\xi}_\mu - \mathbf{x}\| \cdot \|\boldsymbol{\xi}_\mu\| \leq \|\boldsymbol{\xi}_\mu - \mathbf{x}\|m, \tag{B.42}$$

we write $\widetilde{\Delta}_\mu$ in terms of Δ_μ:

$$\widetilde{\Delta}_\mu = \Delta_\mu - 2\|\boldsymbol{\xi}_\mu - \mathbf{x}\|m = \Delta_\mu - 2mR, \qquad \text{(By } \mathbf{x} \in S_\mu\text{)}$$

where R is radius of the sphere S_μ. Since $\mathcal{T}$ is a mapping $\mathcal{T}: S_\mu \to S_\mu$, output of the mapping $\mathcal{T}$ falls in $\mathcal{S}_\mu$ with radius R. Therefore, R is lower-bounded by

$$R \geq (M + k - 2)\exp\{-\beta(\Delta_\mu - 2mR)\}m \geq \|\mathcal{T}(\mathbf{x}) - \boldsymbol{\xi}_\mu\|, \tag{B.43}$$

and thus

$$\Delta_\mu \geq \frac{1}{\beta}\ln\left(\frac{(M + k - 2)m}{R}\right) + 2mR. \tag{B.44}$$

$\square$

B.8 Lemma 4.2

We built our proof on top of [Hu et al., 2023, Lemma 2.1], which consists 3 steps:

- **(Step 1.)** We establish a more refined well-separation condition, ensuring that patterns $\{\boldsymbol{\xi}_\mu\}_{\mu \in [M]}$ are well-stored in $\mathcal{H}$ and can be retrieved by $\mathcal{T}$ with an error ϵ at most R.

- **(Step 2.)** This condition is then related to the cosine similarity of memory patterns, from which we deduce an inequality governing the probability of successful pattern storage and retrieval.

- **(Step 3.)** We pinpoint the conditions for exponential memory capacity and confirm their satisfaction.

Proof of Lemma 4.2. Our proof is built on top of [Hu et al., 2023, Corollary 3.1.1] with a different well-separation condition.

Let $\Delta_{\min} \coloneqq \text{Min}_{\mu \in [M]} \Delta_\mu$ and $\theta_{\mu\nu}$ Here we define $\Delta_{\min}$ and $\theta_{\mu\nu}$ be the angle between two patterns $\boldsymbol{\xi}^\mu$ and $\boldsymbol{\xi}^\nu$.

In order for a pattern $\boldsymbol{\xi}_\mu$ to be well-stored, by Theorem 4.2, we need

$$\Delta_{\min} \geq \frac{1}{\beta} \ln\left(\frac{(M+k-2)m}{R}\right) + 2mR. \tag{B.45}$$

On the other hand, we observe

$$\Delta_{\min} = \underset{1 \leq \mu \leq \nu \leq M}{\text{Min}} \left[m^2 \left(1 - \cos(\theta_{\mu\nu})\right)\right] = m^2 \left[1 - \cos(\theta_{\min})\right], \tag{B.46}$$

where $\theta_{\min} \coloneqq \text{Min}_{1 \leq \mu \leq \nu \leq M} \theta_{\mu\nu} \in [0, \pi]$. Then, we have

$$m^2 \left[1 - \cos(\theta_{\min})\right] \geq \frac{1}{\beta} \ln\left(\frac{(M+k-2)m}{R}\right) + 2mR. \tag{B.47}$$

As a result, the probability of successful storage and retrieval, i.e., the minimal separation $\Delta_{\min}$ that satisfies Theorem 4.2, is given by

$$P\left(\Delta_\mu \geq \frac{1}{\beta} \ln\left(\frac{(M+k-2)m}{R}\right) + 2mR\right) = 1 - p. \tag{B.48}$$

Inserting (B.47) into above, we obtain

$$P\left(m^2\left[1 - \cos(\theta_{\min})\right] \geq \frac{1}{\beta}\ln\left(\frac{(M + k - 2)m}{R}\right) + 2mR\right) = 1 - p. \tag{B.49}$$

From [Olver et al., 2010, Equation (4.22.2)], for $0 \leq \cos(\theta_{\min}) \leq 1$, $\cos(\theta_{\min})$ has an upper bound

$$\cos(\theta_{\min}) \leq 1 - \frac{\theta_{\min}^2}{5}. \tag{B.50}$$

It holds

$$P\left(\frac{m^2\theta_{\min}^2}{5} \geq \frac{1}{\beta}\ln\left(\frac{(M + k - 2)m}{R}\right) + 2mR\right) = 1 - p, \tag{B.51}$$

which leads to

$$P\left(M^{\frac{2}{d-1}}\theta_{\min} \geq \frac{\sqrt{5}M^{\frac{2}{d-1}}}{m}\left[\frac{1}{\beta}\ln\left(\frac{(M + k - 2)m}{R}\right) + 2mR\right]^{\frac{1}{2}}\right) = 1 - p. \tag{B.52}$$

For later convenience, here we introduce an extra $M^{2/d-1}$ on both sides.

Let $\omega_d := \frac{2\pi^{d+1/2}}{\Gamma\left(\frac{d+1}{2}\right)}$ be the area of a d-dimensional unit sphere manifold, with $\Gamma(\cdot)$ denoting the gamma function.

Following [Brauchart et al., 2018, Lemma 3.5], we have

$$P\left(M^{\frac{2}{d-1}}\theta_{\min} \geq \frac{\sqrt{5}M^{\frac{2}{d-1}}}{m}\left[\frac{1}{\beta}\ln\left(\frac{(M + k - 2)m}{R}\right) + 2mR\right]^{\frac{1}{2}}\right) = 1 - p$$

$$\geq 1 - \frac{1}{2}\gamma_{d-1}5^{\frac{d-1}{2}}M^2 m^{-(d-1)}\left[\frac{1}{\beta}\ln\left(\frac{(M + k - 2)m}{R}\right) + 2mR\right]^{\frac{d-1}{2}}, \tag{B.53}$$

where γ_d is the ratio between the surface areas of the unit spheres in $(d - 1)$ and d dimensions:

$$\gamma_d := \frac{1}{d}\frac{\omega_{d-1}}{\omega_d} = \frac{1}{d\sqrt{\pi}}\frac{\Gamma\left(\frac{d+1}{2}\right)}{\Gamma\left(\frac{d}{2}\right)}. \tag{B.54}$$

Recall $d, M \in \mathbb{N}_+$, $p \in [0, 1]$. Hence, it holds $M = \sqrt{p}C^{\frac{d-1}{4}}$ for some real values $C \in \mathbb{R}$.

Then, by (B.53), we have

$$5^{\frac{d-1}{2}} \left(\sqrt{p}C^{\frac{d-1}{4}}\right)^2 m^{-(d-1)} \left\{\frac{1}{\beta}\ln\left[\frac{\left(\sqrt{p}C^{\frac{d-1}{4}}+k-1\right)m}{R}\right]+\frac{1}{\beta}\right\}^{\frac{d-1}{2}} - p \leq 0, \qquad \text{(B.55)}$$

and thus

$$5^{\frac{d-1}{2}} C^{\frac{d-1}{2}} m^{-(d-1)} \left\{\frac{1}{\beta}\ln\left[\frac{\left(\sqrt{p}C^{\frac{d-1}{4}}+k-1\right)m}{R}\right]+\frac{1}{\beta}\right\}^{\frac{d-1}{2}} \leq 1. \qquad \text{(B.56)}$$

Further, we rewrite (B.56) as

$$\frac{5C}{m^2\beta}\left\{\ln\left[\frac{\left(\sqrt{p}C^{\frac{d-1}{4}}+k-1\right)m}{R}\right]+1\right\} - 1 \leq 0, \qquad \text{(B.57)}$$

and identify

$$a := \frac{4}{d-1}\left\{\ln\left[\frac{m(\sqrt{p}+k-1)}{R}\right]+1\right\}, \quad b := \frac{4m^2\beta}{5(d-1)}. \qquad \text{(B.58)}$$

By [Hu et al., 2023, Lemam 3.1], C takes the form

$$C = \frac{b}{W_0(\exp\{a+\ln b\})}, \qquad \text{(B.59)}$$

where $W_0(\cdot)$ is the upper branch of the Lambert W function. Since the domain of the Lambert W function is $x > (-1/e, \infty)$ and the fact $\exp\{a+\ln b\} > 0$, the solution for (B.59) exists.

When the inequality (B.56) holds, the lower bound on the exponential storage capacity M can be written as:

$$M \geq \sqrt{p}C^{\frac{d-1}{4}}. \qquad \text{(B.60)}$$

In particular, the above lower bound takes a form similar to [Ramsauer et al., 2020, Theorem 3].

$\square$

C Nonparametric Modern Hopfield Family

In this section, we derive a family of modern Hopfield models as possible extensions based on the proposed framework (Theorem 3.1). [4]

C.1 Linear Modern Hopfield Model

Proposition C.1 (Linear Modern Hopfield Model). Let $\Phi(\mathbf{x}) = (\phi_1(\mathbf{x}), \dots, \phi_d(\mathbf{x}))$ with the component ϕ:

$$\phi_i(\mathbf{x}) := \frac{\text{elu}(\mathbf{x}[i]) + 1}{\sum_{\mu=1}^{M} \langle \Phi(\mathbf{x}), \Phi(\boldsymbol{\xi}_\mu + \delta\boldsymbol{\xi}_\mu) \rangle}, \quad \forall i \in [d], \tag{C.1}$$

where $\text{elu}(\cdot)$ denotes the exponential linear unit activation function proposed by [Clevert et al., 2015]. By Theorem 3.1, fitting $\mathcal{T}_{\text{SVR}}$ on $\mathcal{D}$ following (3.2) gives

$$\mathcal{T}_{\text{Linear}}(\mathbf{x}) = \frac{\sum_{\mu=1}^{M} \langle \Phi(\mathbf{x}), \Phi(\boldsymbol{\xi}_\mu + \delta\boldsymbol{\xi}_\mu) \rangle \boldsymbol{\xi}_\mu}{\sum_{\nu=1}^{M} \langle \Phi(\mathbf{x}), \Phi(\boldsymbol{\xi}_\nu + \delta\boldsymbol{\xi}_\nu) \rangle}. \tag{C.2}$$

By setting the kernel mapping Φ to linear feature map (C.1), we obtain a **linear modern Hopfield model** with linear complexity $\mathcal{O}(n)$. Compared with dense modern Hopfield model, our proposed linear modern Hopfield model has time and memory complexity $\mathcal{O}(n)$ instead of $\mathcal{O}(n^2)$ since we only need to compute $\sum_{\mu=1}^{M} \Phi(\boldsymbol{\xi}_\mu + \delta\boldsymbol{\xi}_\mu)\boldsymbol{\xi}_\mu$ and $\sum_{\mu=1}^{M} \Phi(\boldsymbol{\xi}_\mu + \delta\boldsymbol{\xi}_\mu)$ once and reuse them for the computation of every query pattern. This model is by design connected to the random attention of linear attention [Katharopoulos et al., 2020].

C.2 Multi-Head Modern Hopfield Models

To derive the multi-head Hopfield model, we cast $\mathcal{T}_{\text{Multi}}$ as multiple SVR problems such that the memorization of memory patterns $\boldsymbol{\Xi}$ corresponds to training a regression model $\mathcal{T}_{\text{Multi}}$ on datasets $\{\boldsymbol{\Xi}_s\}_{s\in[H]}$ with noises $\{\boldsymbol{\Xi}\}$. These S training data sets are given as $\{(\boldsymbol{\xi}_\mu^1 + \delta\boldsymbol{\xi}_\mu^1, \boldsymbol{\xi}_\mu^1)\}_{\mu\in[M]}, \cdots, \{(\boldsymbol{\xi}_\mu^H + \delta\boldsymbol{\xi}_\mu^H, \boldsymbol{\xi}_\mu^H)\}_{\mu\in[M]}$. To handle multiple regression problems, we extend the regression model (3.1) into the following.

Definition C.1 (Multi-Head Regression Model). Given an input vector $\mathbf{x} \in \mathbb{R}^d$. The output

---

[4]Hu et al. [2024b] provide a theoretical characterization of these possible extensions from the perspective of fine-grained complexity theory.

$\hat{\mathbf{y}} \in \mathbb{R}^d$ of the regression model $\mathcal{T}_{\text{multi}}$ is defined as:

$$\hat{\mathbf{y}} = \mathcal{T}_{\text{Multi}}(\mathbf{x}) := \sum_{s=1}^{H} \mathbf{W}_O^s \left(\mathbf{W}^s \Phi^s(\mathbf{x})\right) \in \mathbb{R}^d, \tag{C.3}$$

where $\mathbf{W}_O^s \in \mathbb{R}^{d \times d}$, $\mathbf{W}^s = [\mathbf{w}_1^s, \cdots, \mathbf{w}_d^s]^\mathsf{T} \in \mathbb{R}^{d \times D_\Phi}$ for all $s \in [H]$, and $\Phi^s(\mathbf{x}) = (\phi_1^s(\mathbf{x}), \cdots, \phi_{D_\Phi}^s(\mathbf{x})) : \mathbb{R}^d \to \mathbb{R}^{D_\Phi}$ denote a series of output projection matrices, weighted matrix and kernel mapping, respectively.

Adopting this multi-head regression model, we introduce the following multi-head modern Hopfield model.

Proposition C.2 (Multi-Head Modern Hopfield Models). Let $\Phi(\cdot) = (\phi_0^{(0)}, \phi_1^{(1)}, \ldots, \phi_{D_1}^{(1)}, \ldots, \phi_1^{(n)}, \ldots, \phi_{D_n}^{(n)}, \ldots)$ with, for $1 \leq D' \leq D_n$,

$$\phi_{D'}^{(n)} := \frac{(\sqrt{\beta}x_1)^{\ell_1} \cdots (\sqrt{\beta}x_d)^{\ell_d}}{\sum_{\mu=1}^{M} \langle \Phi(\boldsymbol{\xi}_\mu + \delta\boldsymbol{\xi}_\mu), \Phi(\mathbf{x}) \rangle \cdot \sqrt{\ell_1! \cdots \ell_d!}}, \tag{C.4}$$

where $\ell_1 + \cdots + \ell_d = n$, and $D_n := \binom{d+n-1}{n}$. By Theorem 3.1, fitting $\mathcal{T}_{\text{SVR}}$ on H training data sets $\{(\boldsymbol{\xi}_\mu^1 + \delta\boldsymbol{\xi}_\mu^1, \boldsymbol{\xi}_\mu^1)\}_{\mu \in [M]}, \cdots, \{(\boldsymbol{\xi}_\mu^H + \delta\boldsymbol{\xi}_\mu^H, \boldsymbol{\xi}_\mu^H)\}_{\mu \in [M]}$ following (3.2) gives

$$\mathcal{T}_{\text{Multi}}(\mathbf{x}) = \sum_{s=1}^{H} \mathbf{W}_O^s \left(\boldsymbol{\Xi}_s \operatorname{Softmax}(\beta \boldsymbol{\Xi}_\delta^\mathsf{T} \mathbf{x})\right). \tag{C.5}$$

This model is by design connected to the standard multi-head attention.

C.3   PRFs (Positive Random Features) Kernel Modern Hopfield Model

Proposition C.3 (Positive Random Features Modern Hopfield Model). Let $\Phi(\cdot) = (\phi_1, \ldots, \phi_{D_\Phi})$ with

$$\Phi(\mathbf{x}) := \frac{\Psi(\mathbf{x})}{\sqrt{D_\Phi}}(\psi_1(\langle \mathbf{p}_1, \mathbf{x} \rangle), \ldots, \psi_1(\langle \mathbf{p}_m, \mathbf{x} \rangle), \ldots, \psi_l(\langle \mathbf{p}_1, \mathbf{x} \rangle), \ldots, \psi_l(\langle \mathbf{p}_m, \mathbf{x} \rangle)), \tag{C.6}$$

where $D_\Phi = l \cdot m$, $\Psi : \mathbb{R}^d \to \mathbb{R}$, $\psi_1, \ldots, \psi_m$ are functions that map from $\mathbb{R} \to \mathbb{R}$, and $\mathbf{p}_1, \ldots, \mathbf{p}_m \overset{iid}{\sim} \mathcal{P}$ are vectors from some distribution $\mathcal{P} \in \Delta^d$ ($\Delta^d := \{\mathbf{p} \in \mathbb{R}_+^d \mid \sum_{i=1}^{d} p_i = 1\}$ is the $(d-1)$-dimensional unit simplex.). By Theorem 3.1, fitting $\mathcal{T}_{\text{SVR}}$ on $\mathcal{D}$ following (3.2) gives

$$\mathcal{T}_{\text{PRF}}(\mathbf{x}) = \sum_{\mu=1}^{M} \mathbb{E}_\mathcal{D}[\widehat{D}^{-1} \langle \Phi(\mathbf{x}), \Phi(\boldsymbol{\xi}_\mu + \delta\boldsymbol{\xi}_\mu) \rangle] \boldsymbol{\xi}_\mu, \tag{C.7}$$

where we adopt the normalization map $\widehat{D}^{-1} := \langle \boldsymbol{\xi}_1, \mathbf{x} \rangle$ given by [Choromanski et al., 2021].

Comparing with regular modern Hopfield model, PRF Hopfield model only has the linear space and time complexity, without any additional treatment such as introducing sparsity or low-rankness. The significance of this representational capability lies in its ability to facilitate a precise comparison between softmax and alternative kernels in the context of extensive tasks, surpassing the capabilities of regular modern Hopfield models and enabling a comprehensive exploration of optimal kernels. This model is by design connected to the Performer-type attention [Choromanski et al., 2021]. In practice, the default option for $\mathcal{P}$ is standard Gaussian [Choromanski et al., 2021].

D Nonparametric Modern Hopfield Layers for Deep Learning

Building on the link between the nonparametric modern Hopfield models and the attention mechanisms, we introduce the Nonparametric Hopfield (NPH) layers for deep learning.

Following [Hu et al., 2023, Ramsauer et al., 2020], we say $\mathbf{X}$ and $\mathbf{\Xi}$ are in the associative space (embedded space), as they are embedded from the *raw* query $\mathbf{R}$ and $\mathbf{Y}$ memory patterns, respectively, via $\mathbf{X}^{\mathsf{T}} = \mathbf{R}\mathbf{W}_Q \coloneqq \mathbf{Q}$, and $\mathbf{\Xi}^{\mathsf{T}} = \mathbf{Y}\mathbf{W}_K \coloneqq \mathbf{K}$, with some $\mathbf{W}_Q$ and $\mathbf{W}_K$. Taking the transpose of $\mathcal{T}$ in (3.4) (with a given feature map Φ) and multiplying with $\mathbf{W}_V$ such that $\mathbf{V} \coloneqq \mathbf{K}\mathbf{W}_V$, we have

$$\mathbf{Z} \coloneqq \mathbf{Q}^{\text{new}}\mathbf{W}_V = \mathcal{T}_{\text{SVR}}\left(\beta\mathbf{Q}\mathbf{K}^{\mathsf{T}}\right)\mathbf{V}, \tag{D.1}$$

which leads to an attention mechanisms with various $\mathcal{T}_{\text{SVR}}$ as activation functions. Plugging back the raw patterns $\mathbf{R}$ and $\mathbf{Y}$, we arrive the Nonparametric Modern Hopfield (NPH) layer(s),

$$\text{NPH}\left(\mathbf{R}, \mathbf{Y}\right) = \mathcal{T}_{\text{SVR}}\left(\beta\mathbf{R}\mathbf{W}_Q\mathbf{W}_K^{\mathsf{T}}\mathbf{Y}^{\mathsf{T}}\right)\mathbf{Y}\mathbf{W}_K\mathbf{W}_V, \tag{D.2}$$

which can be seamlessly integrated into deep learning architectures. Concretely, the NPH layers take matrices $\mathbf{R}$, $\mathbf{Y}$ as inputs, with the weight matrices $\mathbf{W}_Q$, $\mathbf{W}_K$, $\mathbf{W}_V$. Depending on its configuration, it offers several functionalities:

1. **Memory Retrieval:** In this learning-free setting, weight matrices $\mathbf{W}_K$, $\mathbf{W}_Q$, and $\mathbf{W}_V$ are set as identity matrices. Here, $\mathbf{R}$ represents the query input, and $\mathbf{Y}$ denotes the stored memory patterns for retrieval.

2. NPH: This configuration takes $\mathbf{R}$ and $\mathbf{Y}$ as inputs. Intending to substitute the attention mechanism, the weight matrices $\mathbf{W}_K$, $\mathbf{W}_Q$, and $\mathbf{W}_V$ are rendered learnable. Furthermore, $\mathbf{R}$, $\mathbf{Y}$, and $\mathbf{Y}$ serve as the sources for query, key, and value respectively. Achieving a self-attention-like mechanism requires setting $\mathbf{R}$ equal to $\mathbf{Y}$.

3. NPHPooling: With inputs $\mathbf{Q}$ and $\mathbf{Y}$, this layer uses $\mathbf{Q}$ as a static **prototype pattern**, while $\mathbf{Y}$ contains patterns over which pooling is desired. Given that the query pattern is replaced by the static prototype pattern $\mathbf{Q}$, the only learnable weight matrices are $\mathbf{W}_K$ and $\mathbf{W}_V$.

4. NPHLayer: The NPHLayer layer takes the query $\mathbf{R}$ as its single input. The layer equips with learnable weight matrices $\mathbf{W}_K$ and $\mathbf{W}_V$, which function as our stored patterns and their corresponding projections. This design ensures that our key and value are decoupled from the input. In practice, we set $\mathbf{W}_Q$ and $\mathbf{Y}$ as identity matrices.

E Experimental Studies

We verify the method proposed in the main content with the following experimental sections.

1. Memory Retrieval Task (Figure 3).

2. Multiple Instance Learning on MNIST (Figure 5).

3. Multiple Instance Learning on Real World Datasets.

4. Time Series Prediction.

5. Computational Efficiency.

We consider the following variations of Modern Hopfield Models in this paper:

- Dense Modern Hopfield [Ramsauer et al., 2020]

- Sparse Modern Hopfield [Hu et al., 2023]

- Sparse-Structured Modern Hopfield:
    - Random Masked Modern Hopfield

    - Window Modern Hopfield

    - Top-K Modern Hopfield
- Linear Modern Hopfield

- Random Feature Modern Hopfield

E.1   Memory Retrieval Task (Figure 3)

In the memory retrieval task, we examine two datasets: MNIST (sparse) and CIFAR10 (dense). We employ the sum-of-squares distance between the retrieved image and the ground truth image to measure retrieval error. This experiment encompasses two settings:

1. Half-masked image recovery, and

2. Noisy image recovery.

In the half-masked image recovery scenario, we obscure half of the pixels in the image. The memory set size (M) is varied from 10 to 200, and we report the average retrieval error (sum-of-square difference) over 50 runs. In the noisy image recovery scenario, we fix the memory set size at 100, and introduce varying scales of Gaussian noise to the image, with variance ranging from 0.1 to 1.4.

Implementation Details. The memory set itself is chosen randomly from the dataset in each iteration. We adhere to the implementation outlined in [Hu et al., 2023].
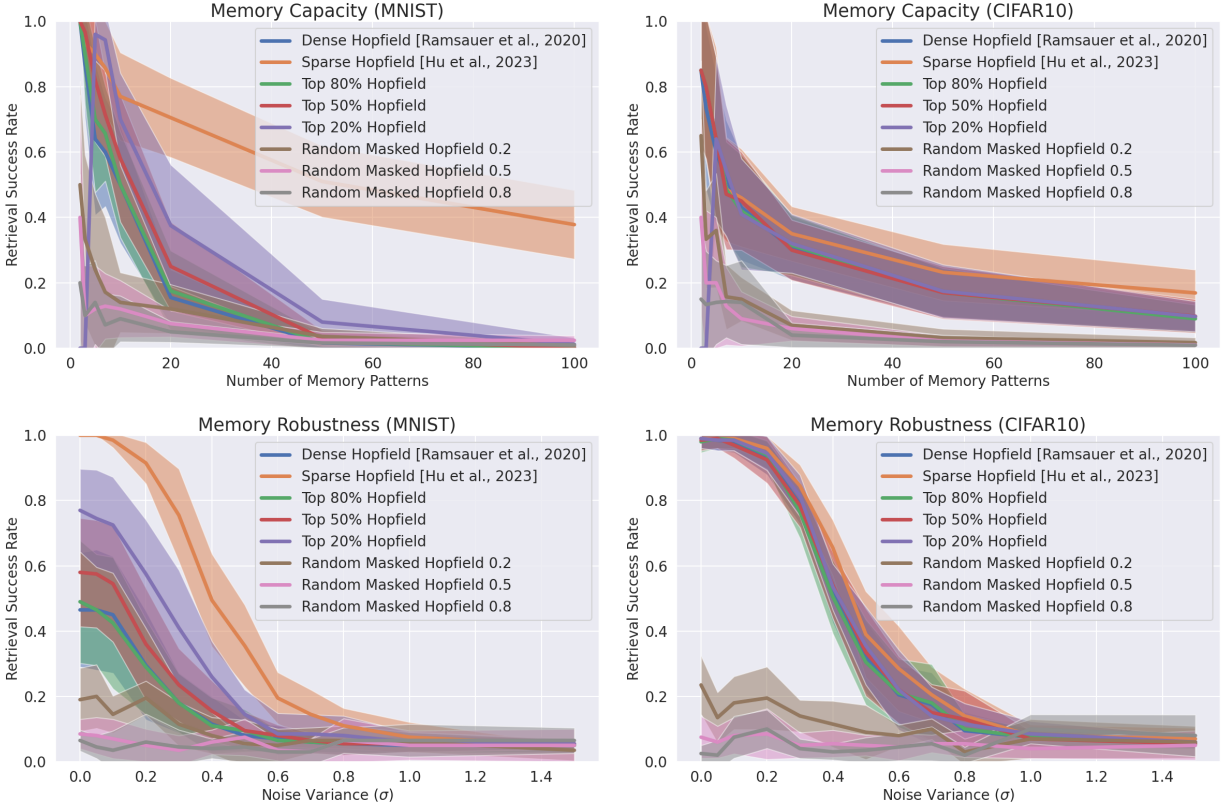
Figure 3: **Numerical Justifications for Theoretical Results: Memory Capacity and Noise Robustness.** (**Upper**): Memory Capacity measured by successful retrieval rates from half-masked queries (Lemma 4.2). (**Bottom**): Memory Robustness measured by success retrieval rates from noisy queries with different scales of Gaussian noise (Remark 4.2). For all Hopfield models, we set $\beta = .01/0.1$ (for MNIST/CIFAR10) for better visualizations. Plotted are the means and standard deviations of 10 runs. We see that Top-K Hopfield shows similar exponential capacity as Dense [Ramsauer et al., 2020] and Sparse Hopfield [Hu et al., 2023]. Note that the Random Masked Hopfield models perform poorly, especially on MNIST. This is because they violate the $\mu \in \mathcal{M}$ assumption in Theorem 3.2, as the random mask might inadvertently mask out the correct pattern in the memory set.

E.2 Multiple Instance Learning on MNIST (Figure 4 & Figure 5)

Multiple Instance Learning (MIL) [Ilse et al., 2018, Carbonneau et al., 2018] is a variation of supervised learning where the training set consists of labeled bags, each containing multiple instances. The goal of MIL is to predict the bag labels based on the instances they contain, which makes it particularly useful in scenarios where labeling individual instances is difficult or impractical, but bag-level labels are available. Examples of such scenarios include medical imaging (where a bag could be an image, instances could be patches of the image, and the label could indicate the presence or absence of disease) and document classification (where a bag could be a document, instances could be the words or sentences in the document, and the label could indicate the topic or sentiment of the document).
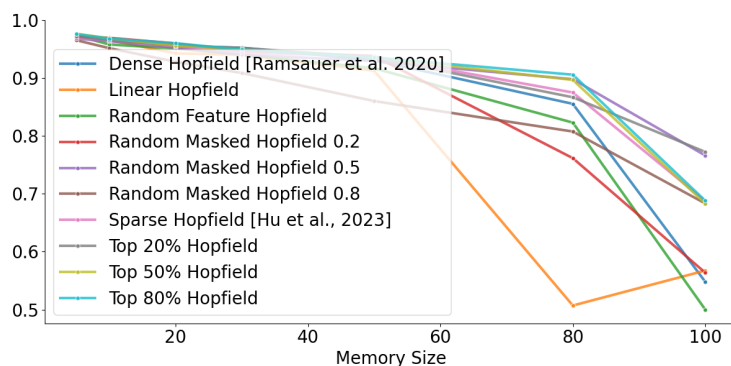

Figure 4:   **Comparison of MIL performance varying bag sizes.** The y-axis represents the accuracy on test set. We employ various variants of the `HopfieldPooling` layers to observe to performance change with respect to different bag size. We see that for those generate actual sparse matrices (Top-K, Random Masked and Sparse Hopfield), their performances are more robust against bag size increase.

In this experiment, we designate one digit from MNIST as a negative signal, and the remaining digits as positive signals. The objective is to predict whether a given bag of instances (digits) contains the negative signal. We vary the memory set size (M) from 5 to 100 and report the mean accuracy over 10 runs. We compare the performance of Dense Hopfield, Sparse Hopfield, Top-K Hopfield (with 20%, 50%, and 80%), Random Feature Hopfield, Random Masked Hopfield and Linear Hopfield. We omit Window Hopfield for reasons mentioned earlier. The result can be found in Figure 4. Additionally, we also conduct a convergence analysis in Figure 5 with bag size = 50. We plot the loss and accuracy curve on MNIST MIL training and test set.

Implementation Details. We employ an embedding layer to project the flattened MNIST images into the hidden space, followed by a layer of layer normalization. Subsequently, we utilize the

Hopfield Pooling layer to pool over all the instances in the bag, followed by a second layer normalization layer. Finally, a fully connected layer is used to project the hidden representation of the bag into the label space. All models are trained using the AdamW optimizer for 150 epochs, with a cosine annealing learning rate decay applied to all models. Note that we exclude Window Hopfield in this and the subsequent MIL experiment since Window Hopfield requires both the query and memory pattern numbers to be large to perform the sliding window operation. However, in our model structure, the number of query patterns in the pooling layer is set to 2. The details of the hyperparameters can be found in Table 2.

Table 2: Hyperparameter used in the MIL MNIST experiment.

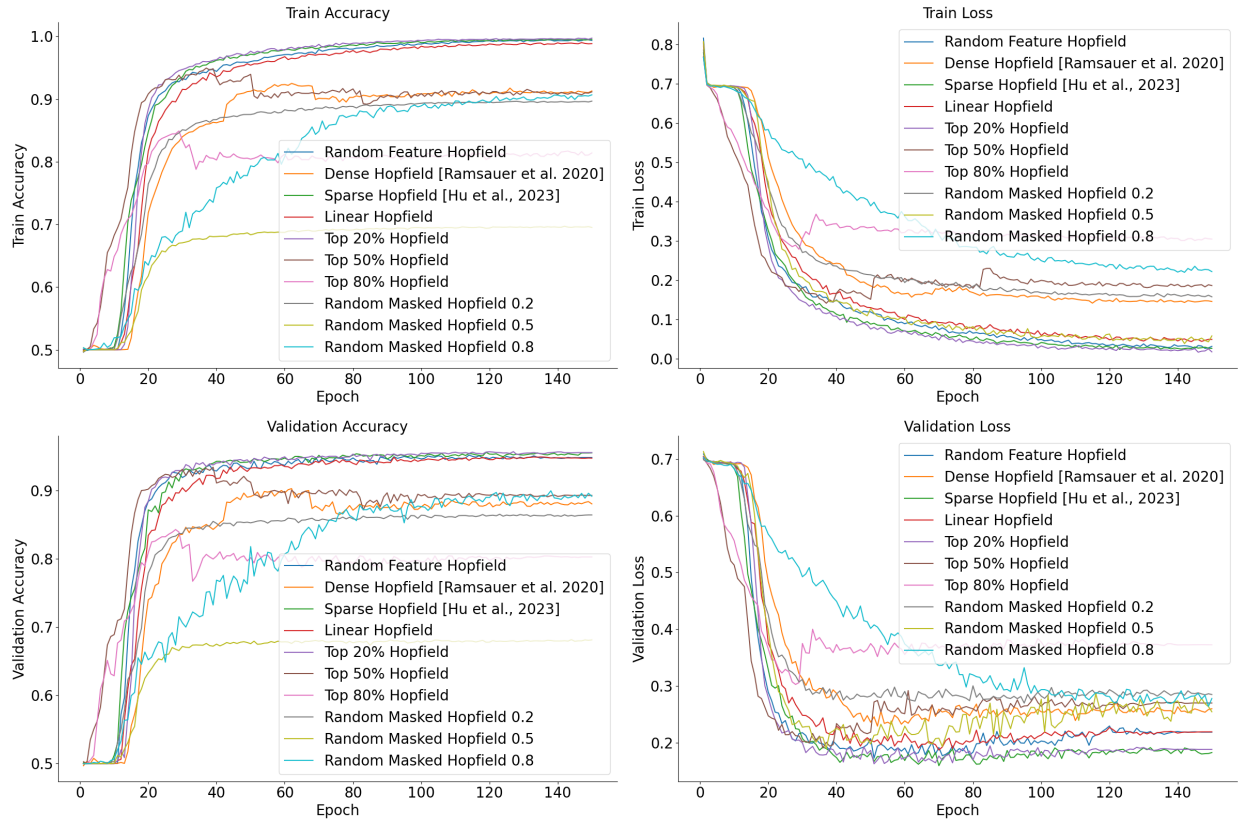| parameter	values
batch size	256
learning rate	1e-3
embedding dimension	256
number of heads	4
head dimension	64
test set size	500
train set size	2000
scaling	0.1
num of pattern	2
epochs	150

Figure 5: **Numerical Justifications for Theoretical Results: Convergence Analysis.** (**Upper**): Training loss and accuracy curve of different Hopfield models on MNIST multiple instance learning task (Theorem 4.1). (**Bottom**): Validation loss and accuracy curve of different Hopfield models on MNIST multiple instance learning task (Theorem 4.1). We train all the model with 150 epochs with cosine annealing learning rate decay. Plotted are the means over 10 runs. We observe that with Sparse Hopfield having the highest validation accuracy, Random feature Hopfield also shows competitive performance with faster convergence speed. On the other hand, Top 20% Hopfield also converges fast with almost no performance drop. More experimental details can be found in Appendix E.

E.3 Multiple Instance Learning on Real World Datasets

For this experiment, we follow [Ramsauer et al., 2020, Hu et al., 2023] to conduct MIL experiments on real world datasets. However, we employ a simpler model structure and a smaller hyperparameter search space, rendering our results incomparable. We utilize four datasets: Elephant, Fox, and Tiger for image annotation [Ilse et al., 2018], and UCSB breast cancer classification [Kandemir et al., 2014]. We compare Dense Hopfield, Sparse Hopfield, TopK Hopfield at 20%, 50%, and 80%, Random Feature Hopfield, and Linear Hopfield. Random Masked Hopfield is excluded due to its non-deterministic inference, and Window Hopfield is omitted as previously mentioned. The results are presented in Table 5.

Dataset Details. The experiment is conducted on four MIL datasets. **Elephant**, **Fox**, and **Tiger** are designed for image annotation and consist of preprocessed and segmented colored images. Each image is characterized by descriptors for color, texture, and shape. These datasets each contain 100 positive images featuring the specified animal and 100 negative images drawn from a set of images depicting other animals. Additionally, we evaluate our model on the **UCSB** breast cancer classification task. In the UCSB dataset, each instance comprises a patch of a histopathological image depicting either cancerous or normal tissue. The detailed statistics of the datasets are reported in Table 3.

Table 3: Statistics of MIL benchmark datasets

Name	Instances	Features	Bags	+bags	−bags
Elephant	1391	230	200	100	100
Fox	1302	230	200	100	100
Tiger	1220	230	200	100	100
UCSB	2002	708	58	26	32

Implementation Details. We follow the experimental setting in [Ramsauer et al., 2020] and employ stratified 10-fold cross-validation to evaluate the performance of each baseline Hopfield model. In each fold, we utilize a stratified sampling process to partition the data into a training set and a validation set, with a split rate of 0.1. Hyperparameters are optimized via random search by maximizing the ROC-AUC score on the validation set. All reported ROC-AUC scores represent the average results over 5 runs with different random seeds. The random search space is delineated in Table 4, with the number of trials set to 50 for each fold. The embedding layer, a pre-HopfieldPooling linear network, has its layer width determined by the number of hidden units. A dropout operation, also referred to as bag dropout, is applied post the embedding layer and the Hopfield Pooling layer. Notably, to better showcase the performance of Top-k Hopfield, dropout is not applied to the attention weight. All models are trained using the Adam optimizer over 50 epochs. To mitigate overfitting, an early-stopping mechanism is employed, selecting the best checkpoint based on the validation set.

46

Table 4: Hyperparameter random search space on the respective validation sets of the Elephant, Fox, Tiger and UCSB breast cancer datasets.

parameter	values
batch size	$\{4, 8, 16\}$
learning rates	$\{10^{-3}, 10^{-4}, 10^{-5}\}$
weight decay	$\{0, 10^{-3}, 10^{-4},\}$
layer width	$\{128, 256, 512\}$
number of heads	$\{4, 8\}$
scaling factors	$\{0.1, 1\}$
dropout	$\{0.0, 0.3\ 0.5\}$

Table 5: Results for MIL benchmark datasets in terms of AUC score. The results suggest that the proposed model achieves performance comparable to the existing Dense and Sparse Modern Hopfield models [Hu et al., 2023, Ramsauer et al., 2020]. Note that, since our aim here is to conduct an *atomic* setting for fair comparison, we employ a simpler network structure (with smaller hyperparameter search space) compared to the ones used in [Hu et al., 2023, Ramsauer et al., 2020]. Consequently, our results do not align with those in [Hu et al., 2023] for Dense and Sparse Modern Hopfield Models.

Method	Tiger	Fox	Elephant	UCSB
Dense Hopfield [Ramsauer et al., 2020]	0.813	0.563	0.877	0.524
Sparse Hopfield [Hu et al., 2023]	0.830	0.573	0.893	0.585
Top-20% Hopfield	0.824	0.562	0.848	0.586
Top-50% Hopfield	0.812	0.566	0.852	0.572
Top-80% Hopfield	0.812	0.560	0.872	0.551
Random Feature Hopfield	0.802	0.508	0.875	0.566
Linear Hopfield	0.797	0.571	0.869	0.561

E.4 Time Series Prediction

We further showcase the performance (in Table 6) and efficiency (in Figure 6) of the proposed nonparametric modern Hopfield models with multivariate time series prediction tasks.

Table 6: **Time series prediction using different Hopfield layers (Appendix D) across five datasets.** We evaluate each dataset with different prediction horizons (showed in the second column). We report the average Mean Square Error (MSE) and Mean Absolute Error (MAE) metrics of 5 runs. **RF** denotes the **R**andom **F**eature Hopfield layer. One notable observation is that the noise level of the dataset significantly influences time series prediction. Therefore, employing Hopfield layers with strong noise-robustness offers performance improvements. Moreover, based on our results, the proposed efficient Hopfield models not only offer significant computational efficiency but also maintain comparable performance. Especially, the Random Feature Hopfield and Linear Hopfield layers (models) not only match but even outperform Dense Hopfield model in several settings. As a side note, Window Hopfield exhibits significant performance degradation in most settings. This degradation arises because it solely focuses on local information. Being the only Hopfield model that does not span the entire associative range (i.e., sequence length), it overlooks a substantial portion of the autoregressive correlation present in time series data. We also record the time used for one epoch on ETTh1 dataset with different prediction horizon (input length as well). The duration time per epoch was showed in Figure 6.

Models		Dense		Sparse		Top20%		Top50%		Top80%		Window		RF		Linear	
Metric		MSE	MAE	MSE	MAE	MSE	MAE	MSE	MAE	MSE	MAE	MSE	MAE	MSE	MAE	MSE	MAE
ETTh1	96	0.137	0.307	0.144	0.314	0.148	0.319	0.153	0.321	0.147	0.318	1.043	0.881	0.147	0.312	0.149	0.320
	192	0.153	0.326	0.152	0.325	0.146	0.318	0.161	0.333	0.150	0.320	1.003	0.870	0.158	0.332	0.141	0.313
	336	0.148	0.319	0.146	0.319	0.156	0.327	0.122	0.286	0.160	0.333	0.889	0.767	0.151	0.322	0.138	0.307
	720	0.169	0.331	0.148	0.314	0.184	0.345	0.161	0.327	0.123	0.287	0.756	0.761	0.141	0.271	0.171	0.333
ETTm1	96	0.148	0.301	0.147	0.301	0.144	0.311	0.151	0.310	0.142	0.31o	0.943	0.854	0.151	0.314	0.155	0.319
	192	0.189	0.350	0.187	0.340	0.191	0.347	0.185	0.338	0.188	0.341	1.054	0.893	0.190	0.347	0.192	0.348
	336	0.163	0.320	0.165	0.322	0.168	0.331	0.161	0.312	0.169	0.330	0.873	0.334	0.175	0.333	0.176	0.337
	720	0.159	0.300	0.161	0.303	0.165	0.313	0.167	0.313	0.169	0.320	0.764	0.731	0.162	0.309	0.165	0.310
ECL	96	0.378	0.371	0.373	0.370	0.384	0.382	0.386	0.386	0.383	0.376	0.989	0.854	0.390	0.403	0.365	0.378
	192	0.486	0.426	0.535	0.507	0.502	0.427	0.501	0.464	0.519	0.481	1.000	0.843	0.543	0.438	0.549	0.464
	336	0.748	0.693	0.760	0.688	0.650	0.549	0.674	0.571	0.638	0.545	1.012	0.849	0.767	0.588	0.672	0.578
	720	0.961	0.711	0.993	0.758	1.145	0.843	1.166	0.847	1.211	0.872	1.061	0.865	1.362	0.896	1.052	0.770
WTH	96	0.347	0.474	0.347	0.477	0.348	0.474	0.348	0.474	0.356	0.479	0.952	0.819	0.345	0.470	0.355	0.476
	192	0.399	0.505	0.386	0.497	0.360	0.482	0.370	0.490	0.361	0.482	0.977	0.828	0.368	0.487	0.354	0.478
	336	0.407	0.512	0.387	0.501	0.376	0.489	0.397	0.503	0.403	0.505	0.931	0.808	0.392	0.504	0.407	0.514
	720	0.669	0.631	0.632	0.623	0.590	0.604	0.569	0.593	0.618	0.618	0.564	0.595	0.564	0.595	0.747	0.676
Traffic	96	1.466	0.654	1.489	0.638	1.483	0.645	1.517	0.630	1.477	0.638	1.520	0.625	1.515	0.635	1.489	0.644
	192	1.551	0.654	1.550	0.657	1.557	0.649	1.548	0.657	1.551	0.652	1.570	0.637	1.551	0.654	1.551	0.653
	336	1.595	0.663	1.595	0.662	1.599	0.663	1.592	0.665	1.604	0.657	1.612	0.646	1.613	0.646	1.614	0.646
	720	1.660	0.681	1.671	0.671	1.664	0.674	1.676	0.663	1.682	0.661	1.683	0.661	1.682	0.661	1.681	0.660

E.4.1 Implementation Details

For ease of comparison, we employ the simplest possible architecture: an embedding layer to project each signal into a hidden space, followed by a single Hopfield layer. By doing so, we treat every signal as a query pattern. Next, we employ a Hopfield Pooling layer to pool over all

the signals into a single hidden vector. Finally, we utilize a fully connected layer to generate the prediction. For all experiments, we maintain the same input and prediction horizon for simplicity. The results can be found in Table 6 and Figure 6.

Datasets. We conduct the experiments on four multivariate time series real-world datasets: ETTh1 (Electricity Transformer Temperature-hourly), ETTm1 (Electricity Transformer Temperature-minutely), WTH (Weather), ECL (Electricity Consuming Load), Traffic.

Setup. For each dataset, we use their univariate setting for our time series prediction experiment. We choose Dense, Sparse, Random Feature, Linear, TopK and Window Hopfield as baselines. We select 4 different prediction horizons for demonstration, which are $96, 196, 336, 720$. We report the average error of 5 runs, evaluated using Mean Square Error (MSE) and Mean Absolute Error (MAE) metrics. For window Hopfield, we set the window size as $8, 12, 14, 16$, w.r.t. $96, 196, 336, 720$.
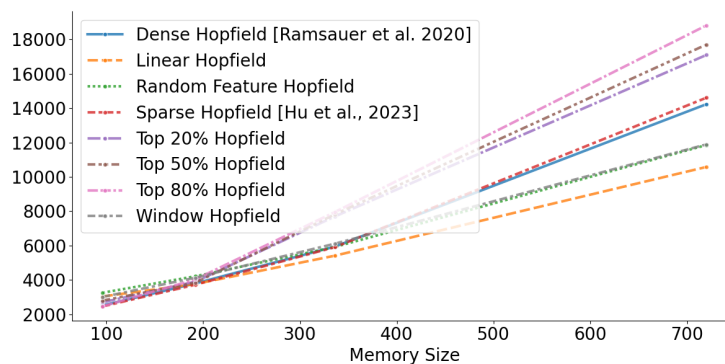
Figure 6: The processing time comparison among different Hopfield models utilized in the time series prediction task described in Table 6. We evaluate the efficiency of multivariate time series prediction on ETTh1 dataset. The findings are consistent with the efficiency discussion in Section 3.2, where the Sparse/Dense/Top-K models (all with $\mathcal{O}(d^2)$ complexity) necessitate more time to complete an epoch. In conjunction with the results in Figure 5, it is evident that the efficient modern Hopfield models (Window, Linear, Random Feature) not only converge in fewer or comparable epochs but also require less time per epoch compared to the less efficient (Sparse/Dense/Top-K) Hopfield models.

E.5   Computational Efficiency

Here we demonstrate the computational overhead for different efficient modern Hopfield variants. We focus on the computational time duration and Flops (the number of Floating point operations). The results demonstrate

- For random masked Hopfield, the computational time scales up with respect to probability.

- Random feature Hopfield, Linear Hopfield and Window Hopfield demonstrates fast computational overhead in practice. In addition, these efficient Hopfield models also enjoy significantly lower floating point operations with only a marginal sacrifice in performance.

- Under PyTorch (version 1.11.0) framework, random masked Hopfield is not able to obtain computational efficiency improvement despite from its sparse-structured nature.
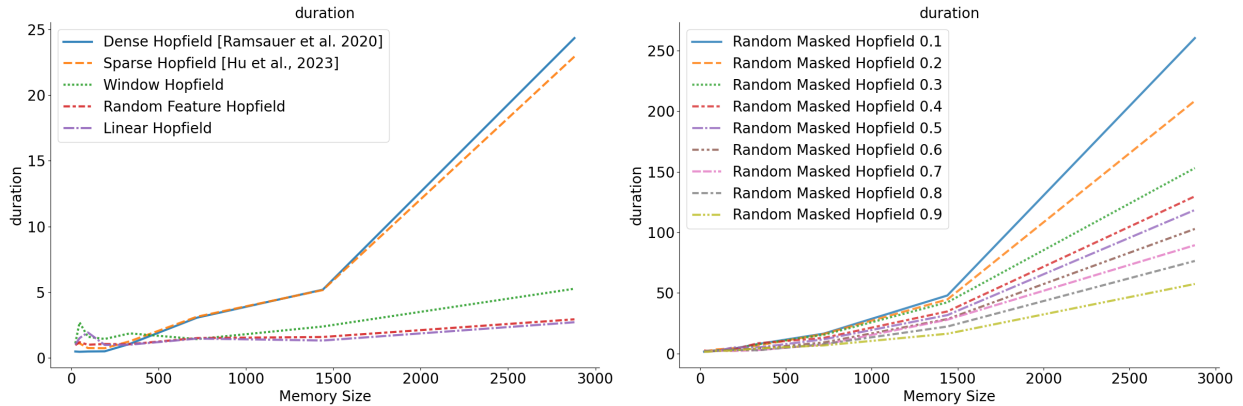

Figure 7: **(LHS:)** Comparison of duration (ms) per batch for different Hopfield Models. **(RHS:)** The scaling behavior of Random Masked Hopfield with different masking ratios. The probability denotes the ratio being masked out. We employ various variants of the `Hopfield` layers to process a batch of tensors, with a batch size of 4 and a hidden dimension of 16. We vary the input memory size (input length). Note that we separate the Random Masked Hopfield from other baselines since the sparse matrix operation in PyTorch, still in the beta stage, may not be as fully optimized as dense tensor operations.

Implementation Details. In this section, we exclusively evaluate the computational efficiency of different Hopfield models with respect to varying input lengths using the *Hopfield* layer. We report the average duration time per batch, as shown in Figure 7, and the FLOPs concerning different input lengths (memory sizes), as depicted in Figure 8. It's notable that different code implementation methods could potentially affect computational efficiency. We use a randomized batched tensor as input x, where $x \in \mathbb{R}^{\text{memory size} \times 16}$, and the batch size is 4 [5]. For Random Feature

---

[5]approximately $(4 \times 4 \times 16 \times \text{memory size})$ bytes
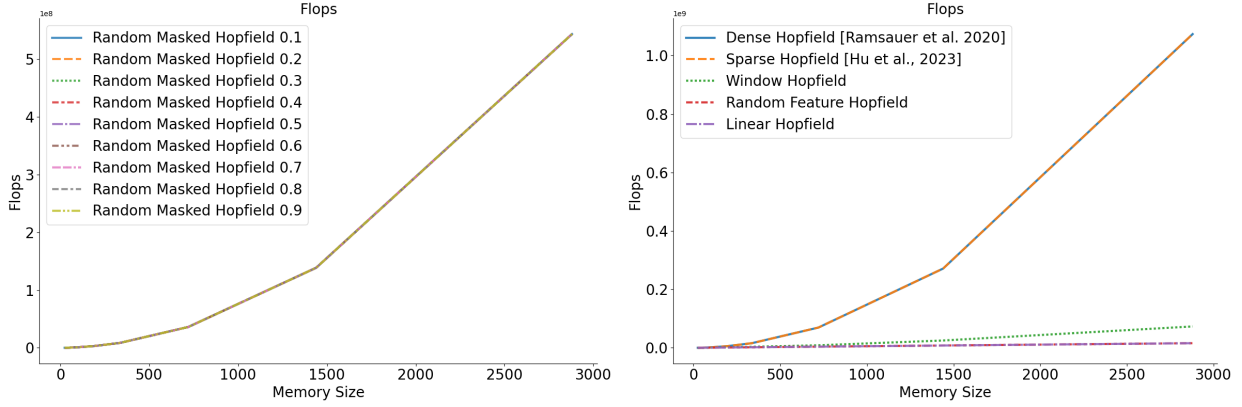
Figure 8: **(LHS:)** The FLOPs comparison for Random Masked Hopfield with different probabilities is depicted. The lines for Dense and Sparse Hopfield are overlapped, as are the lines for Random Feature Hopfield and Linear Hopfield. **(RHS:)** The FLOPs comparison across different Hopfield Models is shown. We employ the same settings as in the duration figure. Note that the **fvcore** package may count sparse matrix operations as normal floating point operations, which is why we might not see a difference.

Hopfield and Linear Hopfield, we adhere to the Performer implementation[6], while for Window Hopfield, we follow the Longformer implementation[7]. For Random Masked Hopfield, we utilize the `torch.sparse.sampled_addmm`[8] feature, and for other baselines, we employ standard PyTorch built-in functions for implementation. We report the average forward pass time over 10 runs, alongside the FLOPs, with both metrics evaluated on different input lengths. FLOPs are calculated using the **fvcore** package[9]. Note that most publicly available packages for FLOPs profiling are either under development or in beta, hence calculation errors are anticipated. Additionally, the `torch.sparse` package is also in beta, implying its performance may not be fully optimized, especially regarding FLOPs calculation and operation overhead.

Discussion. Note that, by nature, both Dense and Sparse Hopfield exhibit the same FLOPs. Moreover, it is observed that Random Feature Hopfield and Linear Hopfield also share the same FLOPs, as the only distinction between them lies in the kernel function. Regarding Window Hopfield, its FLOPs fall in between, demonstrating notable efficiency compared to both Dense and Sparse Hopfield. In terms of duration time per batch, Sparse Hopfield appears slightly faster than its dense counterpart, likely due to the additional zeros generated by sparsemax. Window Hopfield, on the other hand, showcases a significant reduction in duration compared to Sparse Hopfield. Lastly, it is noted that the processing time for both Random Feature Hopfield and Linear Hopfield converges as the memory size increases.

---

[6]https://github.com/lucidrains/performer-pytorch

[7]https://github.com/allenai/longformer

[8]https://pytorch.org/docs/stable/generated/torch.sparse.sampled_addmm.html#torch.sparse.sampled_addmm

[9]https://github.com/facebookresearch/fvcore

References

Andreas Auer, Martin Gauch, Daniel Klotz, and Sepp Hochreiter. Conformal prediction for time series with modern hopfield networks. *Advances in Neural Information Processing Systems*, 36, 2024. URL https://arxiv.org/abs/2303.12783.

Mariette Awad, Rahul Khanna, Mariette Awad, and Rahul Khanna. Support vector regression. *Efficient learning machines: Theories, concepts, and applications for engineers and system designers*, pages 67–80, 2015. URL https://link.springer.com/chapter/10.1007/978-1-4302-5990-9_4.

Iz Beltagy, Matthew E Peters, and Arman Cohan. Longformer: The long-document transformer. *arXiv preprint arXiv:2004.05150*, 2020. URL https://arxiv.org/abs/2004.05150.

Rishi Bommasani, Drew A Hudson, Ehsan Adeli, Russ Altman, Simran Arora, Sydney von Arx, Michael S Bernstein, Jeannette Bohg, Antoine Bosselut, Emma Brunskill, et al. On the opportunities and risks of foundation models. *arXiv preprint arXiv:2108.07258*, 2021. URL https://arxiv.org/abs/2108.07258.

Johannes Brandstetter. Blog post: Hopfield networks is all you need, 2021. URL https://ml-jku.github.io/hopfield-layers/. Accessed: April 4, 2023.

Johann S Brauchart, Alexander B Reznikov, Edward B Saff, Ian H Sloan, Yu Guang Wang, and Robert S Womersley. Random point sets on the sphere-hole radii, covering, and separation. *Experimental Mathematics*, 27(1):62–81, 2018. URL https://arxiv.org/abs/1512.07470.

Tom Brown, Benjamin Mann, Nick Ryder, Melanie Subbiah, Jared D Kaplan, Prafulla Dhariwal, Arvind Neelakantan, Pranav Shyam, Girish Sastry, Amanda Askell, et al. Language models are few-shot learners. *Advances in neural information processing systems*, 33:1877–1901, 2020. URL https://proceedings.neurips.cc/paper_files/paper/2020/hash/1457c0d6bfcb4967418bfb8ac142f64a-Abstract.html?utm_medium=email&utm_source=transaction.

Marc-André Carbonneau, Veronika Cheplygina, Eric Granger, and Ghyslain Gagnon. Multiple instance learning: A survey of problem characteristics and applications. *Pattern Recognition*, 77:329–353, 2018.

Degang Chen, Qiang He, and Xizhao Wang. The infinite polynomial kernel for support vector machine. In *Advanced Data Mining and Applications: First International Conference, ADMA 2005, Wuhan, China, July 22-24, 2005. Proceedings 1*, pages 267–275. Springer, 2005. URL https://link.springer.com/chapter/10.1007/11527503_32.

Rewon Child, Scott Gray, Alec Radford, and Ilya Sutskever. Generating long sequences with sparse transformers. *arXiv preprint arXiv:1904.10509*, 2019. URL https://arxiv.org/abs/1904.10509

Krzysztof Marcin Choromanski, Valerii Likhosherstov, David Dohan, Xingyou Song, Andreea Gane, Tamas Sarlos, Peter Hawkins, Jared Quincy Davis, Afroz Mohiuddin, Lukasz Kaiser, David Benjamin Belanger, Lucy J Colwell, and Adrian Weller. Rethinking attention with performers. In *International Conference on Learning Representations*, 2021. URL https://openreview.net/forum?id=Ua6zuk0WRH.

Djork-Arné Clevert, Thomas Unterthiner, and Sepp Hochreiter. Fast and accurate deep network learning by exponential linear units (elus). *arXiv preprint arXiv:1511.07289*, 2015. URL https://arxiv.org/abs/1511.07289.

Gonçalo M Correia, Vlad Niculae, and André FT Martins. Adaptively sparse transformers. *arXiv preprint arXiv:1909.00015*, 2019. URL https://arxiv.org/abs/1909.00015.

Mete Demircigil, Judith Heusel, Matthias Löwe, Sven Upgang, and Franck Vermet. On a model of associative memory with huge storage capacity. *Journal of Statistical Physics*, 168:288–299, 2017. URL https://link.springer.com/article/10.1007/s10955-017-1806-y.

Yichuan Deng, Zhao Song, and Tianyi Zhou. Superiority of softmax: Unveiling the performance edge over linear attention. *arXiv preprint arXiv:2310.11685*, 2023.

Luciano Floridi and Massimo Chiriatti. Gpt-3: Its nature, scope, limits, and consequences. *Minds and Machines*, 30:681–694, 2020. URL https://link.springer.com/article/10.1007/s11023-020-09548-1.

Andreas Fürst, Elisabeth Rumetshofer, Johannes Lehner, Viet T Tran, Fei Tang, Hubert Ramsauer, David Kreil, Michael Kopp, Günter Klambauer, Angela Bitto, et al. Cloob: Modern hopfield networks with infoloob outperform clip. *Advances in neural information processing systems*, 35:20450–20468, 2022. URL https://arxiv.org/abs/2110.11316.

Ankit Gupta, Guy Dar, Shaya Goodman, David Ciprut, and Jonathan Berant. Memory-efficient transformers via top-k attention. *arXiv preprint arXiv:2106.06899*, 2021. URL https://arxiv.org/abs/2106.06899.

Benjamin Hoover, Yuchen Liang, Bao Pham, Rameswar Panda, Hendrik Strobelt, Duen Horng Chau, Mohammed J Zaki, and Dmitry Krotov. Energy transformer. *arXiv preprint arXiv:2302.07253*, 2023. URL https://arxiv.org/abs/2302.07253.

John J Hopfield. Neural networks and physical systems with emergent collective computational abilities. *Proceedings of the national academy of sciences*, 79(8):2554–2558, 1982. URL https://www.pnas.org/doi/abs/10.1073/pnas.79.8.2554.

John J Hopfield. Neurons with graded response have collective computational properties like those of two-state neurons. *Proceedings of the national academy of sciences*, 81(10):3088–3092, 1984. URL https://www.pnas.org/doi/abs/10.1073/pnas.81.10.3088.

Jerry Yao-Chieh Hu, Donglin Yang, Dennis Wu, Chenwei Xu, Bo-Yu Chen, and Han Liu. On sparse modern hopfield model. In *Thirty-seventh Conference on Neural Information Processing Systems*, 2023. URL https://arxiv.org/abs/2309.12673.

Jerry Yao-Chieh Hu, Pei-Hsuan Chang, Robin Luo, Hong-Yu Chen, Weijian Li, Wei-Po Wang, and Han Liu. Outlier-efficient hopfield layers for large transformer-based models. 2024a.

Jerry Yao-Chieh Hu, Thomas Lin, Zhao Song, and Han Liu. On computational limits of modern hopfield models: A fine-grained complexity analysis. *arXiv preprint arXiv:2402.04520*, 2024b.

Maximilian Ilse, Jakub Tomczak, and Max Welling. Attention-based deep multiple instance learning. In *International conference on machine learning*, pages 2127–2136. PMLR, 2018. URL https://arxiv.org/abs/1802.04712.

Martin Jaggi. An equivalence between the lasso and support vector machines. *Regularization, optimization, kernels, and support vector machines*, pages 1–26, 2014. URL https://arxiv.org/abs/1303.1152.

Yanrong Ji, Zhihan Zhou, Han Liu, and Ramana V Davuluri. Dnabert: pre-trained bidirectional encoder representations from transformers model for dna-language in genome. *Bioinformatics*, 37(15):2112–2120, 2021. URL https://academic.oup.com/bioinformatics/article/37/15/2112/6128680?login=false.

Melih Kandemir, Chong Zhang, and Fred A Hamprecht. Empowering multiple instance histopathology cancer diagnosis by cell graphs. In *Medical Image Computing and Computer-Assisted Intervention–MICCAI 2014: 17th International Conference, Boston, MA, USA, September 14-18, 2014, Proceedings, Part II 17*, pages 228–235. Springer, 2014. URL https://link.springer.com/chapter/10.1007/978-3-319-10470-6_29.

Angelos Katharopoulos, Apoorv Vyas, Nikolaos Pappas, and François Fleuret. Transformers are rnns: Fast autoregressive transformers with linear attention. In *International conference on machine learning*, pages 5156–5165. PMLR, 2020. URL https://proceedings.mlr.press/v119/katharopoulos20a.html.

Feyza Duman Keles, Pruthuvi Mahesakya Wijewardena, and Chinmay Hegde. On the computational complexity of self-attention. In *International Conference on Algorithmic Learning Theory*, pages 597–619. PMLR, 2023.

Leo Kozachkov, Ksenia V Kastanenka, and Dmitry Krotov. Building transformers from neurons and astrocytes. *bioRxiv*, pages 2022–10, 2022. URL https://www.pnas.org/doi/abs/10.1073/pnas.2219150120.

Dmitry Krotov and John J Hopfield. Dense associative memory for pattern recognition. *Advances in neural information processing systems*, 29, 2016. URL https://proceedings.neurips.cc/paper_files/paper/2016/hash/eaae339c4d89fc102edd9dbdb6a28915-Abstract.html.

Dmitry Krotov and John J. Hopfield. Large associative memory problem in neurobiology and machine learning. In *International Conference on Learning Representations*, 2021. URL https://arxiv.org/abs/2008.06996.

Andre Martins and Ramon Astudillo. From softmax to sparsemax: A sparse model of attention and multi-label classification. In *International conference on machine learning*, pages 1614–1623. PMLR, 2016. URL https://arxiv.org/abs/1602.02068.

Andre F. T. Martins, Vlad Niculae, and Daniel McNamee. Sparse modern hopfield networks. *Associative Memory & Hopfield Networks in 2023. NeurIPS 2023 workshop.*, 2023. URL https://openreview.net/pdf?id=zwqlV7HoaT.

Frank WJ Olver, Daniel W Lozier, Ronald F Boisvert, and Charles W Clark. *NIST handbook of mathematical functions hardback and CD-ROM*. Cambridge university press, 2010. URL https://dlmf.nist.gov/.

Fabian Paischer, Thomas Adler, Vihang Patil, Angela Bitto-Nemling, Markus Holzleitner, Sebastian Lehner, Hamid Eghbal-Zadeh, and Sepp Hochreiter. History compression via language models in reinforcement learning. In *International Conference on Machine Learning*, pages 17156–17185. PMLR, 2022. URL https://proceedings.mlr.press/v162/paischer22a.html.

Jiezhong Qiu, Hao Ma, Omer Levy, Scott Wen-tau Yih, Sinong Wang, and Jie Tang. Blockwise self-attention for long document understanding. *arXiv preprint arXiv:1911.02972*, 2019. URL https://arxiv.org/abs/1911.02972.

Hubert Ramsauer, Bernhard Schafl, Johannes Lehner, Philipp Seidl, Michael Widrich, Thomas Adler, Lukas Gruber, Markus Holzleitner, Milena Pavlovic, Geir Kjetil Sandve, et al. Hopfield networks is all you need. *arXiv preprint arXiv:2008.02217*, 2020. URL https://arxiv.org/abs/2008.02217.

Johannes Schimunek, Philipp Seidl, Lukas Friedrich, Daniel Kuhn, Friedrich Rippmann, Sepp Hochreiter, and Günter Klambauer. Context-enriched molecule representations improve few-shot drug discovery. In *The Eleventh International Conference on Learning Representations*, 2023. URL https://openreview.net/forum?id=XrMWUuEevr.

Philipp Seidl, Philipp Renz, Natalia Dyubankova, Paulo Neves, Jonas Verhoeven, Jorg K Wegner, Marwin Segler, Sepp Hochreiter, and Gunter Klambauer. Improving few-and zero-shot reaction template prediction using modern hopfield networks. *Journal of chemical information and modeling*, 62(9):2111–2120, 2022. URL https://pubs.acs.org/doi/full/10.1021/acs.jcim.1c01065.

Bharath K Sriperumbudur and Gert RG Lanckriet. On the convergence of the concave-convex procedure. In *Advances in neural information processing systems*, volume 9, pages 1759–1767, 2009. URL https://papers.nips.cc/paper_files/paper/2009/file/8b5040a8a5baf3e0e67386c2e3a9b903-Paper.pdf.

Yi Tay, Mostafa Dehghani, Dara Bahri, and Donald Metzler. Efficient transformers: A survey. *ACM Computing Surveys*, 55(6):1–28, 2022. URL https://dl.acm.org/doi/10.1145/3530811.

Ashish Vaswani, Noam Shazeer, Niki Parmar, Jakob Uszkoreit, Llion Jones, Aidan N Gomez, Łukasz Kaiser, and Illia Polosukhin. Attention is all you need. *Advances in neural information processing systems*, 30, 2017. URL https://proceedings.neurips.cc/paper_files/paper/2017/hash/3f5ee243547dee91fbd053c1c4a845aa-Abstract.html.

Martin J Wainwright. *High-dimensional statistics: A non-asymptotic viewpoint*, volume 48. Cambridge university press, 2019.

Michael Widrich, Bernhard Schäfl, Milena Pavlović, Hubert Ramsauer, Lukas Gruber, Markus Holzleitner, Johannes Brandstetter, Geir Kjetil Sandve, Victor Greiff, Sepp Hochreiter, et al. Modern hopfield networks and attention for immune repertoire classification. *Advances in Neural Information Processing Systems*, 33:18832–18845, 2020. URL https://proceedings.neurips.cc/paper/2020/hash/da4902cb0bc38210839714ebdcf0efc3-Abstract.html.

Dennis Wu, Jerry Yao-Chieh Hu, Teng-Yun Hsiao, and Han Liu. Uniform memory retrieval with larger capacity for modern hopfield models. 2024a.

Dennis Wu, Jerry Yao-Chieh Hu, Weijian Li, Bo-Yu Chen, and Han Liu. STanhop: Sparse tandem hopfield model for memory-enhanced time series prediction. In *The Twelfth International Conference on Learning Representations*, 2024b. URL https://arxiv.org/abs/2312.17346.

Shijie Wu, Ozan Irsoy, Steven Lu, Vadim Dabravolski, Mark Dredze, Sebastian Gehrmann, Prabhanjan Kambadur, David Rosenberg, and Gideon Mann. Bloomberggpt: A large language model for finance. *arXiv preprint arXiv:2303.17564*, 2023. URL https://arxiv.org/abs/2303.17564.

Chenwei Xu, Yu-Chao Huang, Jerry Yao-Chieh Hu, Weijian Li, Ammar Gilani, Hsi-Sheng Goan, and Han Liu. Bishop: Bi-directional cellular learning for tabular data with generalized sparse modern hopfield model. 2024.

Manzil Zaheer, Guru Guruganesh, Kumar Avinava Dubey, Joshua Ainslie, Chris Alberti, Santiago Ontanon, Philip Pham, Anirudh Ravula, Qifan Wang, Li Yang, et al. Big bird: Transformers for longer sequences. *Advances in neural information processing systems*, 33:17283–17297, 2020. URL https://proceedings.neurips.cc/paper/2020/hash/c8512d142a2d849725f31a9a7a361ab9-Abstract.html.

Zhihan Zhou, Yanrong Ji, Weijian Li, Pratik Dutta, Ramana V Davuluri, and Han Liu. DNABERT-2: Efficient foundation model and benchmark for multi-species genomes. In *The Twelfth International Conference on Learning Representations*, 2024a. URL https://openreview.net/forum?id=oMLQB4EZE1.

Zhihan Zhou, Winmin Wu, Harrison Ho, Jiayi Wang, Lizhen Shi, Ramana V Davuluri, Zhong Wang, and Han Liu. Dnabert-s: Learning species-aware dna embedding with genome foundation models. *arXiv preprint arXiv:2402.08777*, 2024b. URL https://arxiv.org/abs/2402.08777.